2012

Investigation of hydrocarbon speciation in diesel low-temperature combustion

Kelvin Xie
University of Windsor

INVESTIGATION OF HYDROCARBON SPECIATION IN DIESEL LOW-TEMPERATURE COMBUSTION

by

Kelvin Xie

A Thesis
Submitted to the Faculty of Graduate Studies
through Mechanical, Automotive, and Materials Engineering
in Partial Fulfillment of the Requirements for
the Degree of Master of Applied Science at the
University of Windsor

Windsor, Ontario, Canada

2012

Library and Archives Canada

Published Heritage Branch

395 Wellington Street
Ottawa ON K1A 0N4
Canada

Bibliothèque et Archives Canada

Direction du Patrimoine de l'édition

395, rue Wellington
Ottawa ON K1A 0N4
Canada

Your file Votre référence
ISBN: 978-0-494-83469-5

Our file Notre référence
ISBN: 978-0-494-83469-5

DECLARATION OF ORIGINALITY

I hereby certify that I am the sole author of this thesis and that no part of this thesis has been published or submitted for publication.

I certify that, to the best of my knowledge, my thesis does not infringe upon anyone's copyright nor violate any proprietary rights and that any ideas, techniques, quotations, or any other material from the work of other people included in my thesis, published or otherwise, are fully acknowledged in accordance with the standard referencing practices. Furthermore, to the extent that I have included copyrighted material that surpasses the bounds of fair dealing within the meaning of the Canada Copyright Act, I certify that I have obtained a written permission from the copyright owner(s) to include such material(s) in my thesis and have included copies of such copyright clearances to my appendix.

I declare that this is a true copy of my thesis, including any final revisions, as approved by my thesis committee and the Graduate Studies office, and that this thesis has not been submitted for a higher degree to any other University or Institution.

ABSTRACT

Requirements to meet stringent nitrogen oxide emission regulations are forcing modern diesel engines to adopt low-temperature combustion modes. However, as emission control techniques such as exhaust gas recirculation are implemented to achieve low-temperature combustion, the resulting increase in partial-combustion products can be significant in quantity as pollutants and as sources of lost engine efficiency. This work examined the partial-combustion hydrocarbon species emitted in a research diesel engine operating under low-temperature combustion. The measurement of carbon related emissions were performed using: a flame-ionization detector for total hydrocarbons, a Fourier transform infrared spectrometer for speciation of key hydrocarbons, and non-dispersive infrared detectors for carbon monoxide and carbon dioxide. The quantity and composition of the hydrocarbon emissions with respect to engine load, exhaust gas recirculation rate, intake pressure, and fuel injection pressure were investigated. The results indicated that at low engine loads, heavier hydrocarbons were the dominant contributors to total emissions. At higher loads the shift toward emissions of lighter hydrocarbons, especially in the one to two carbon range, indicated more complete fuel breakdown but lack of complete oxidation.

ACKNOWLEDGEMENTS

The work presented in this manuscript was made possible through the combined contributions of many current and former research associates. I would like to thank Dr. Raj Kumar, Dr. Clarence Mulenga, Dr. Usman Asad, Xiaoye Han, and Yuyu Tan for their previous work setting up the engine test cell. I would like to thank Dr. Meiping Wang for her role in procuring the analytical equipment. I would like to thank Xiaoye Han for his help running the engine experiments detailed in this manuscript. I would like to thank Xiaoye Han and Tongyang Gao for their assistance in setting up the hydrocarbon emissions sampling system. I would like to thank all my colleagues, Dr. Meiping Wang, Dr. Usman Asad, Xiaoye Han, Marko Jeftic, Fangfang Lin, Dr. Shui Yu, Tongyang Gao, Xiaoxi Zhang, and Prasad Divekar for the things they have taught me though our many insightful discussions.

I am immensely thankful for the guidance of my primary advisor, Dr. Ming Zheng, and his influence on my intellectual and professional development. In addition, I am thankful to Dr. Xiang Chen, Dr. Jimi Tjong, and Dr. Graham T. Reader for their advisory roles to this work.

TABLE OF CONTENTS

LIST OF TABLES

LIST OF FIGURES

LIST OF TERMS AND ABBREVIATIONS

λ	Excess air ratio
θ	Engine crank position
abs	Absolute
ATDC	After top dead centre
BDC	Bottom dead centre
CA_5	Crank angle of 5% heat release
CA_{50}	Crank angle of 50% heat release
CAD	Crank angle degree
CR	Compression ratio
CRP	Common-rail pressure
EGR	Exhaust gas recirculation
FID	Flame ionization detector
FSN	Filter smoke number
FTIR	Fourier transform infrared
g/kW•h	Unit of quantity normalized by engine work output
HC	Hydrocarbon
IMEP	Indicated mean effective pressure
MAF	Mass air flow
η	Indicated thermal efficiency

ppb	Parts per billion
ppm	Parts per million
RPM	Revolutions per minute
TDC	Top dead centre
THC	Total hydrocarbon

PREFACE

Combustion has been a transformative technology for mankind. For hundreds of millennia, deep past the veils of recorded history, it has provided us with warmth and illumination, broadened our available diet, and fashioned our tools. In the last three hundred years the great potential of combustion was unleashed to provide us an abundant source of mechanical power. In addressing key issues we face today — energy availability, the impact of fossil fuel use on the climate, and atmospheric pollutants — research in combustion is eminently relevant. This thesis is a modest contribution to the area of diesel low-temperature combustion, specifically the measurement of hydrocarbon species emitted under low-NOx conditions. In Chapter 1, the background and motivation to this research, in terms of emission regulations, engine technology, and the phenomenon of combustion is introduced. A review of pertinent research by other investigators is presented in Chapter 2. The engine and measurement equipment and test conditions are detailed in Chapter 3. The results of the measurement program are presented in Chapter 4. Finally, Chapter 5 summarizes the key findings, followed by recommendations for further investigations.

1. INTRODUCTION

1.1 Historical Background of the Diesel Engine

The Industrial Revolution was a great catalyst for engine technology. The need for power greater than that horses could provide and more flexible than river-bound waterwheels stimulated the invention of the steam engine. The thermal efficiency of the James Watt era steam engine was refined to approximately 4% in 1800 [1]. Greater understanding of the thermodynamics of engines led engineers away from using steam as an intermediate working fluid and to the direct combustion of fuels in the working fluid. The modern internal combustion engine was invented by Nicolaus Otto in 1876 in the form of the four-stroke engine. Early Otto four-stroke engines achieved thermal efficiencies of 17%, a vast improvement over what was possible in steam engines [1]. The next milestone was the "rational heat-engine" envisioned by Rudolph Diesel and first built in 1893 [2]. The essential features of traditional diesel engine are 1) high compression temperatures, above the igniting-point of the fuel being used, giving reliable ignition across a wide range of conditions, 2) subsequent introduction of fuel into the air charge to control the combustion timing, and 3) high expansion ratios to extract work from the heated working fluid. Today, the diesel engine continues to be a prime mover in a wide range of stationary and automotive applications.

1.2 Modern Emissions Regulations

One of the primary drives for diesel technology innovation in the last several decades has been the regulation of engine pollutants. The 1970 *Clean Air Act* established the US Environmental Protection Agency (EPA) with the authority to regulate motor vehicle pollution. The US EPA sets National Ambient Air Quality Standards (NAAQS) for air pollutants that may endanger the public health and welfare. Current NAAQS exist for carbon monoxide, lead, nitrogen dioxide, particulate matter, ozone, and sulphur dioxide. The regulatory approach to reduce the contribution of mobile emissions has been to enforce emission standards on new vehicles and engines [3].

In Canada, the *Motor Vehicle Safety Act* of 1970 provided the legislative authority of national emissions regulations to Transport Canada. National on-road vehicle standards have been in place since 1971. The responsibility for regulating emissions from on-road vehicles was transferred to Environment Canada under the *Canadian Environmental Protection Act* of 1999. Since 1988, Canada has adopted a policy of harmonization of vehicle emissions requirements with the US EPA. This policy has produced a common market with the United States with respect to emissions control technology [4].

A key target of regulatory policies has been the control of ozone levels. Ozone production in the troposphere is formed from atmospheric oxygen in sun-light driven reactions. In polluted areas volatile organic compounds (VOC) and nitrogen oxides

(NOx) serve as precursors and greatly increase the rate of ozone formation. The reaction proceeds with the oxidation of NO to NO_2 by VOCs. The photolysis of NO_2 yields a NO molecule and a ground-state oxygen atom. The ground-state oxygen atom subsequently reacts with molecular oxygen to form ozone. The EPA monitored median of the mean daily maximum eight-hour average ozone concentration from the years 2000 to 2004 was 49 ppb (parts per billion). Peak one-hour averages in urban areas may be significantly higher (for example 200 ppb in Houston, Texas; 170 ppb in Los Angeles, California). Current evidence holds ozone as a cause to decreased lung function, increased airway responsiveness (leading to increased occurrences of asthma and pulmonary inflammation), and likely to be a cause in increasing mortality [5]. Two key initiatives to reduce ozone levels have been to reduce NOx and VOC emissions. Of these pollutants, the greatest challenge for diesel engines has been the reduction of nitrogen oxides [6].

NOx is produced in engines by the reaction of atmospheric nitrogen with oxygen at elevated temperatures. The rate of NOx production only becomes significant above 1800 K, thus much effort is directed at limiting combustion temperatures in engines [6]. Figure 1-1 shows the tightening of NOx standards for heavy-duty diesel engines from the year 1985 to 2010 by 98% to 0.2 g/hp hr. The latest emissions-complaint engines emit NOx in the tens of parts per million (ppm) range. Diesel engines operating without NOx control can emit NOx in excess of 1000 ppm. Urban ambient NOx is commonly at the level of the tens of parts per billion [7].

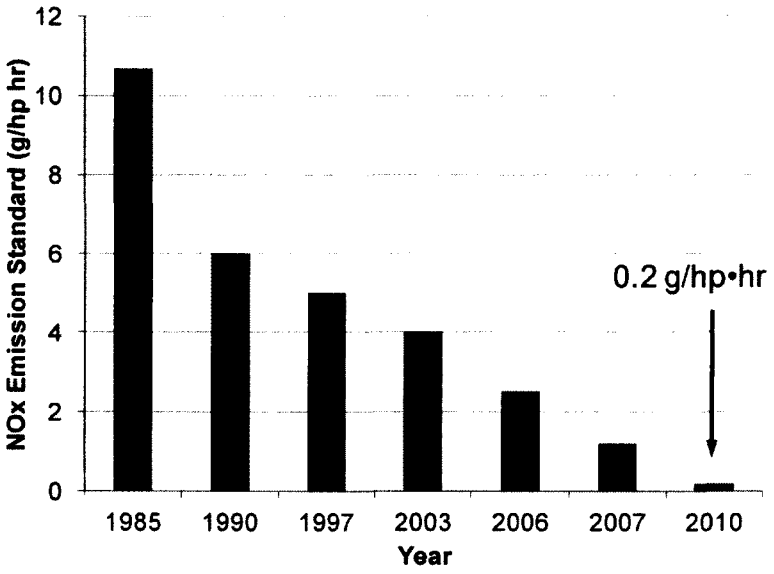

Figure 1-1: US heavy-duty emissions standards for NOx

1.3 State of Diesel Engine Technology

The modern diesel engine utilizes several key technologies to meet emission requirements:

Turbocharging- using a turbine to extract energy from the hot engine exhaust, additional air can be drawn into the engine by a compressor coupled to the turbine. This can be used to increase engine load, to reduce smoke and incomplete combustion products, or enable higher rates of exhaust gas recirculation.

Exhaust gas recirculation (EGR)- replacing a portion of the intake charge with exhaust gas. This has the effect of lowering the intake oxygen and introducing carbon dioxide

into the air charge. The lower oxygen content directly lowers NOx production and extends the ignition delay of the fuel. Carbon dioxide has a higher heat capacity than other major components of air. It has greater ability to absorb the combustion heat, thus lowering the flame temperature.

Intercooler and EGR cooler- using heat exchangers to cool the air charge after the compressor stage and the recirculated exhaust, the air charge density can be increased and the compression temperature decreased. The cooling can provide significant NOx reduction benefit.

High-pressure electronic fuel injection- using high-pressure injections to disperse the fuel into the cylinder air charge can lead to better mixing and less soot production. This in turn allows more EGR to be used for NOx control. High air-fuel homogeneity prior to ignition can directly lead to lower NOx production if sufficient local dilution is available to lower the flame temperature. The combustion temperature can also be lowered if the combustion is phased to occur later in the expansion stroke. Delaying the combustion phasing potentially reduces the temperature and NOx production at the cost of lowering the thermal efficiency of the engine. Electronic injectors have the flexibility of variable injection timing, duration, and the number of injection events.

After-treatment system- when the in-cylinder combustion control strategies cannot effectively or efficiently meet engine-out emissions requirements, additional measures may be taken in the after-treatment system. Hydrocarbons and carbon monoxide may be oxidized by a diesel oxidation catalyst. Particulate matter may be trapped by a diesel

particulate filter. NOx may be treated by selective catalytic reduction or NOx-trap devices.

The air management system of an engines incorporating turborcharging technology and exhaust gas recirculation is illustrated in Figure 1-2. In the configuration presented, the boosted engine intake is provided by a single-stage turbocharger and a portion of the engine exhaust upstream of the turbine is routed back into the engine intake after being cooled in a heat exchanger. Figure 1-3 shows a common-rail fuel management system where a single high-pressure pump supplies fuel to the individual injectors via a common-rail distributor. Figure 1-4 shows the configuration of a 2011 heavy-duty truck after-treatment system that utilizes a first-stage combination diesel oxidation catalyst (DOC) and diesel particulate filter (DPF) to meet hydrocarbon, carbon monoxide, and particulate matter emissions requirements, and a second-stage urea selective catalytic reduction (SCR) system to meet NOx emission requirements.

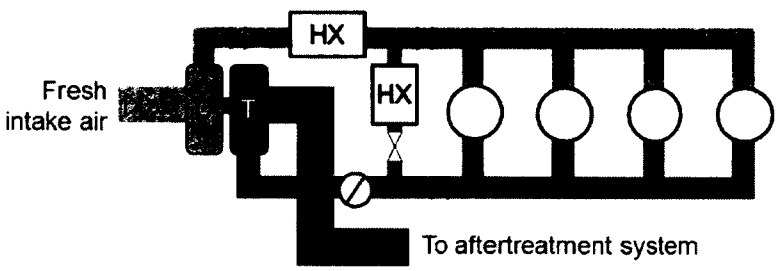

Figure 1-2: Air management in a modern diesel engine

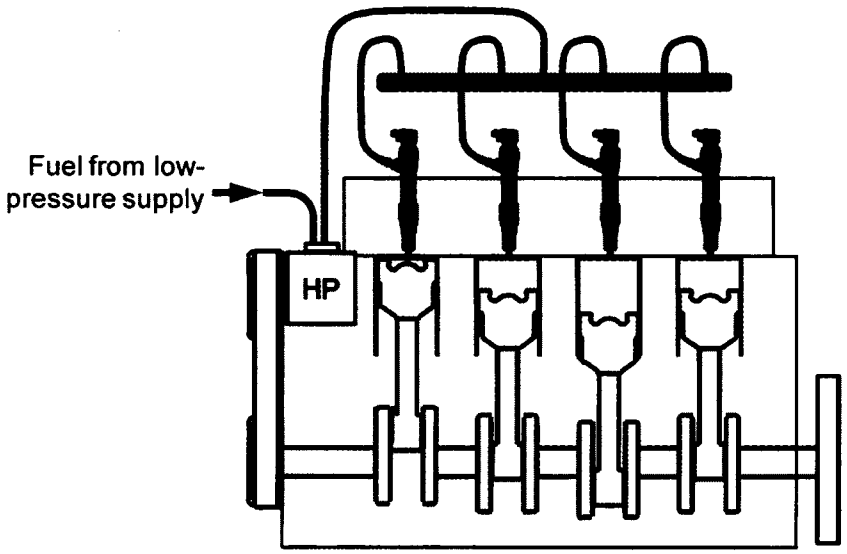

Figure 1-3: A schematic of a common-rail fuel system in a modern diesel engine

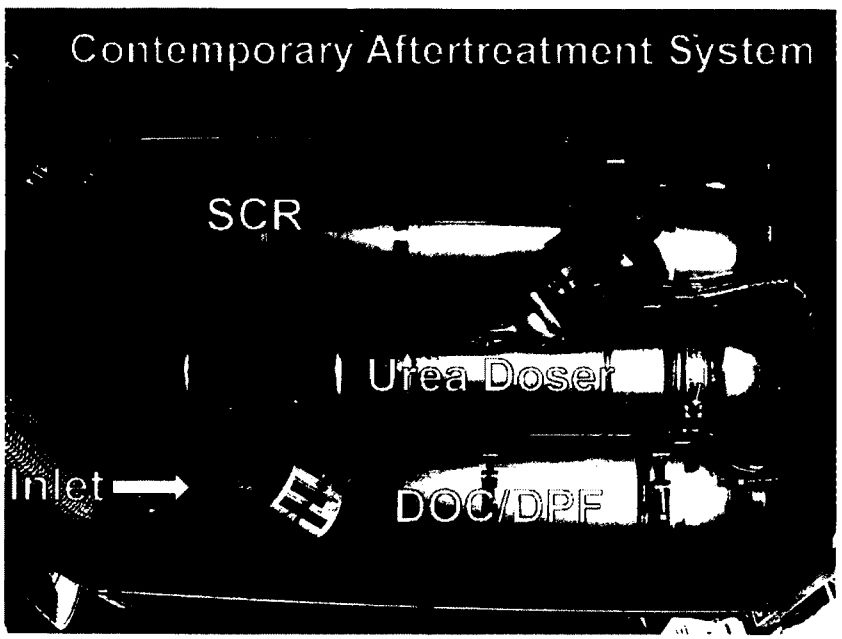

Figure 1-4: A heavy-duty truck after-treatment system with DOC/DPF and SCR

1.4 The Diesel Engine Cycle

The combustion chamber volume of a modern diesel engine is formed by the cylinder head on the top, the recessed bowl of the piston on the bottom, and the cylinder bore in the radial direction. The piston, linked to the engine crank-shaft by a connecting rod and crank-arm, sweeps up and down the cylinder bore as the engine crankshaft rotates. A schematic of the piston and crank mechanism is shown in Figure 1-5 below. The cylinder volume with respect to the engine crank-arm angular position, θ, follows the relation:

$$V(\theta) = V_d \times \left(\frac{1}{CR-1} + 0.5 \times \left(1 + \frac{l}{a} - \cos(\theta) - \left(\left(\frac{l}{a}\right)^2 - sin^2(\theta) \right)^{1/2} \right) \right)$$

where l is the connecting rod length, a is half the engine stroke length, CR is the engine compression ratio, and V_d is the cylinder displacement volume. The cylinder displacement volume is the product of the bore area and the stroke length. The compression ratio is the ratio of the maximum to minimum cylinder volume. Conventionally, θ is referenced from the axis formed by the crank-shaft and the piston. At a θ of zero crank angle degrees (CAD), the piston is at its top-most position and the cylinder volume is at a minimum. This position is known as the piston top-dead centre (TDC) position. As θ increase to 180° CAD, the piston moves to its bottom-most position and the cylinder volume is at its maximum. The relevant engine cycle is defined

by four of such strokes of the piston through the cylinder occurring over two revolutions of the crank. In the intake stroke, an intake valve is opened to draw in fresh air charge into the cylinder as the piston moves downward (θ from 0 to 180° CAD). In the compression stroke (θ from 180 to 360° CAD), the intake valve closes and the charge is compressed. The charge is expanded in the expansion stroke (θ from 360 to 540° CAD). Finally, the charge is expelled from the cylinder by holding open an exhaust valve while the piston moves upward (θ from 540 to 720° CAD).

The compression and expansion of the cylinder charge approximates the isentropic relation:

$$pV^{\gamma} = constant$$

where p is the pressure in the cylinder, V is volume cylinder, and γ is the isentropic ratio of the heat capacities $\frac{c_p}{c_v}$. The conditions of one point of an isentropic process can be used to define subsequent points by the relation:

$$p_0 V_0^{\gamma} = p_1 V_1^{\gamma}$$

The mean gas temperature in the cylinder is approximated by the ideal gas law:

$$pV = mRT$$

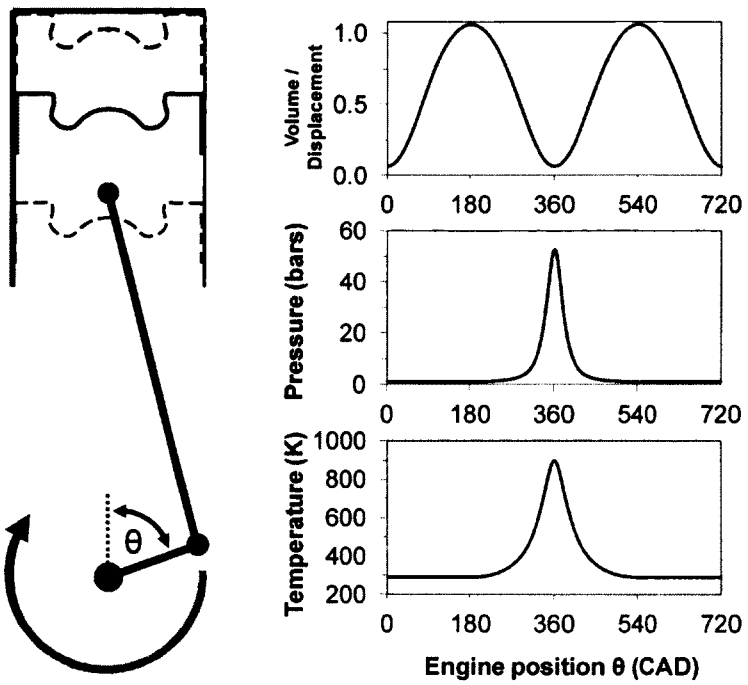

Figure 1-5: Schematic of the piston / crank mechanism

A computed motored engine cycle, using the isentropic and ideal gas relations, is shown in Figure 1-5 to illustrate the effects of compression on the pressure and temperature of an air charge. With a compression ratio of 17:1, the cylinder charge is compressed from ambient conditions to a pressure of 52 bars and temperature of 890 K. In diesel engines, the high temperature is utilized to vaporize and ignite the fuel. The heat released by the combustion of the fuel raises the pressure of the working fluid. Expansion of the working fluid converts the combustion thermal energy into work, which is transferred to the engine crank-shaft. The limit to the thermodynamic efficiency of this process is dependent on the degree of expansion possible. Figure 1-6 plots this efficiency

limit for a range of expansion ratios. In engine designs that have symmetrical compression and expansion ratios, gains in cycle efficiency by increasing the expansion ratio have a consequence of higher cylinder pressures and temperatures. High in-cylinder pressures are a mechanical design issue while high temperatures shorten the ignition delay and potentially lead to higher NOx production.

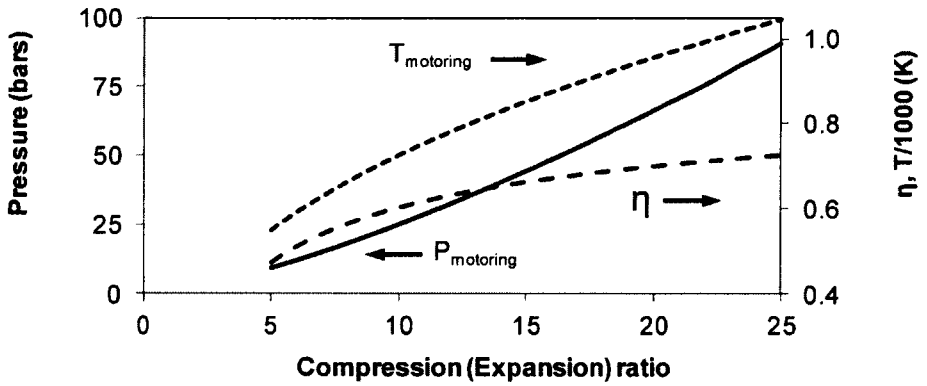

Figure 1-6: Effects of compression ratio on engine cycle parameters

Figure 1-7 shows the thermodynamic properties of a computed cycle with heat released at 358 through 370° CAD, causing the cylinder pressure to increase to 76 bars. The loop seen in the pressure-volume diagram is the result of the departure of the expansion stroke from the compression stroke due to combustion. The area of the loop is proportional to the indicated cycle work. The term *indicated* work refers to the PV work performed by the working fluid. This is in contrast with *brake* work, which is work available at the engine crank-shaft after friction and consumption by auxiliary engine equipment (such as cooling fan, fuel pump, oil pump, valve cams, etc) are subtracted

from the indicated work. A measure of the indicated cycle work normalized to the engine displacement size is the *indicated mean effective pressure* (IMEP). The IMEP of an engine is calculated by the expression:

$$IMEP = \frac{\int_{0°}^{720°} PdV}{V_d}$$

IMEP represents the engine load and is conventionally expressed in bars. The IMEP of the cycle shown in Figure 1-7 is 3.5 bars, a light load condition for modern engines. High-load limits for turbocharged heavy-duty diesel engines are typically in excess of 20 bars IMEP.

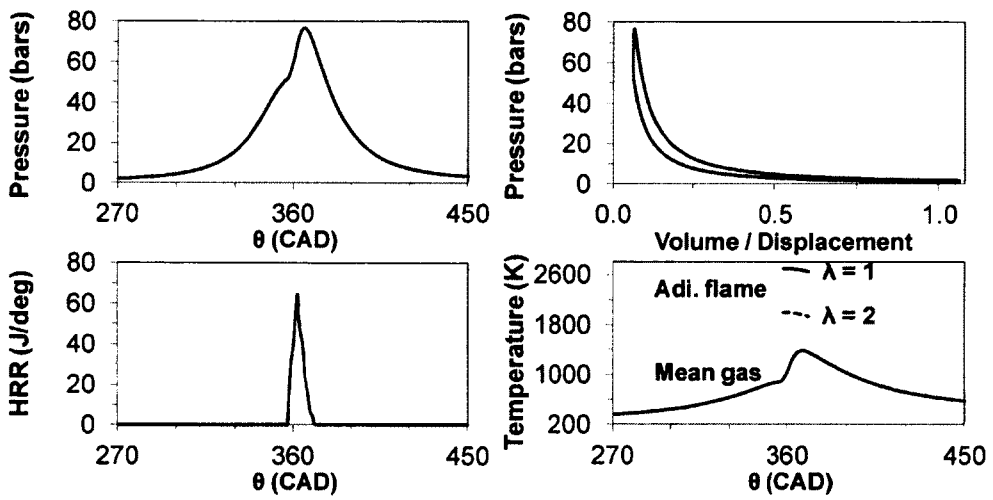

Figure 1-7: Thermodynamic properties of a simulated engine cycle at 3.5 bar IMEP

1.5 Combustion Chemistry

Diesel fuel is a distilled petroleum product that is a blend of various hydrocarbons with a typical size from C_8 (a hydrocarbon molecule having eight carbon atoms) to C_{20}, with the precise composition dependant on the crude oil source and refining process. The light end of the hydrocarbons consists mainly of mono-aromatic benzene derivatives. Substituted benzene derivatives are also present up to C_{20}, but paraffins (hydrocarbon molecules whose carbon to carbon bonds are only single bonds) are dominant in middle and high end hydrocarbons (C_{12} to C_{20}). Di-aromatic naphthalene derivatives are also present in small quantities in the C_{10} to C_{20} range [8]. Examples of these hydrocarbon molecules and their mass fraction are shown in Figure 1-8. Overall, the paraffins, at approximately 70% or higher carbon fraction, account for the majority fuel constituents and are the most influential on the ignition behaviour of diesel fuel [9].

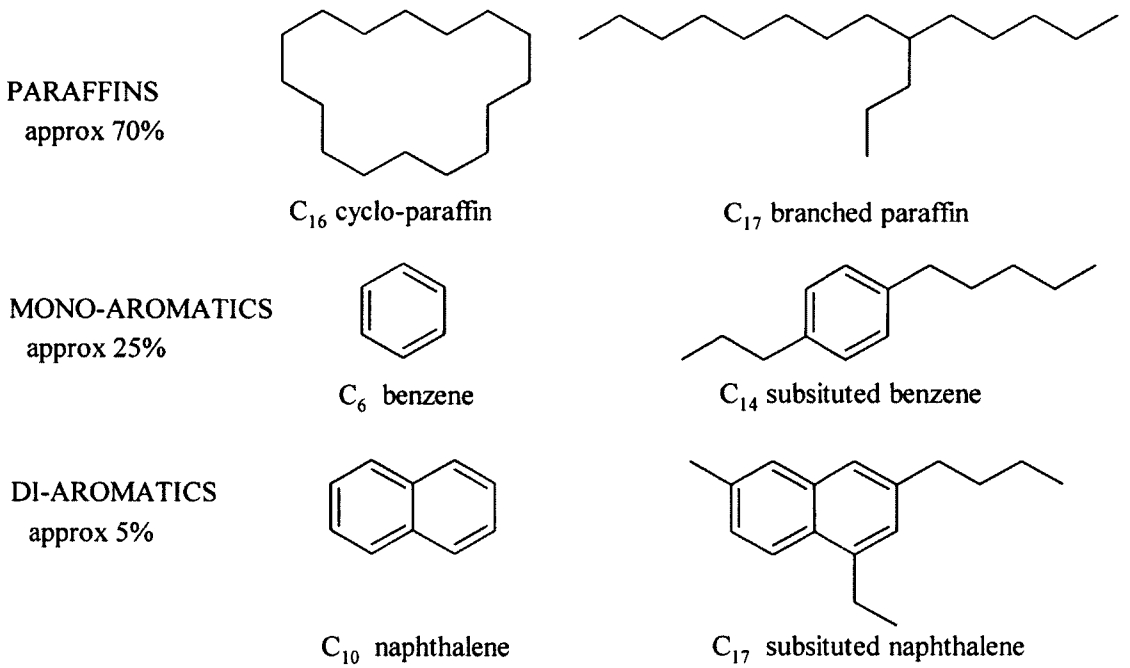

Figure 1-8: Examples of diesel fuel hydrocarbon molecules

Due to the fact that diesel fuel is a blend of hydrocarbons, the stoichiometry of the overall combustion reaction is conventionally written as the reaction of CH_n with air, with n representing the average number of hydrogen atoms per carbon atom. The diesel fuel used in this work has a n value of 1.89. The stoichiometry of the complete combustion of this fuel with air is the following:

$$CH_{1.89}+1.47\times(O_2+3.76N_2) \longrightarrow CO_2+0.945\ H_2O+5.52\ N_2$$

When the ratio of oxygen is exactly sufficient to convert all the fuel into carbon dioxide and water, the fuel-air mixture is *stoichiometric.* When the oxygen is in excess, the mixture is *lean.* When the oxygen is deficient, the mixture is *rich.* The degree of oxygen

availability is conventionally expressed by the terms equivalence ratio (Φ) or excess-air ratio (λ):

$$\Phi = \frac{oxygen_{stoichiometric}}{oxygen_{actual}} \qquad \lambda = \frac{oxygen_{actual}}{oxygen_{stoichiometric}}$$

In practice, even if excess oxygen is present globally, combustion in engines may not go to completion due to deficient local oxygen levels or deficient kinetics at lower temperature levels. The consequence of incomplete combustion is the emission of fuel hydrocarbons, partially reacted hydrocarbons, carbon monoxide, and hydrogen gas.

A chemistry mechanism is a set of elementary chemical reactions that describe a more complex multi-step process, such as combustion. A representative mechanism for diesel oxidation is shown in Figure 1-9 through Figure 1-11, compiled from [6, 9, 10, 11, 12, 13, and 14]. Heptane (C_7) is shown as a surrogate for the larger paraffins that comprise the bulk of diesel fuel. Due to their structural similarities, the reactions of heptane are representative of the reactions of straight-chain paraffins, cyclic paraffins, and the substituted branches of aromatics [10].

The initiation reaction involves the abstraction of a hydrogen atom from heptane (represented by R) by an oxygen molecule, producing an alkyl radical and a hydroperoxyl radical:

$$RH + O_2 \longrightarrow R\cdot + HO_2\cdot$$

The hydroperoxyl radical may abstract an additional hydrogen atom, then decompose, and subsequently produce two hydroxyl radicals:

$$RH+HO_2\cdot \longrightarrow R\cdot+H_2O_2$$

$$H_2O_2 \longrightarrow 2\ OH\cdot$$

Molecular oxygen may also dissociate to produce two oxygen radicals:

$$O_2 \longrightarrow 2\ O\cdot$$

The radicals $HO_2\cdot$, $OH\cdot$, $O\cdot$, and $H\cdot$ produced by the above primary reactions and subsequent secondary reactions abstract hydrogen atoms from additional fuel molecules. The growth of the number of radicals is important in the acceleration of the fuel consumption reactions. The alkyl radicals produced undergo two different pathways depending on the temperature regime. At temperatures above 850 to 900 K, the alkyl radical undergoes β scission to produce an *olefin* (a molecule with a carbon to carbon double bond) and a smaller alkyl radical. At lower temperatures, O_2 addition produces a peroxyl alkyl radical, which subsequently isomerizes to produce hydroperoxyl alkyl radicals. The hydroperoxyl alkyl radical may decompose to produce an olefin and a hydroperoxyl alkyl radical. Alternately, the addition of an O_2 molecule to the hydroperoxyl alkyl radical leads to the formation of a peroxyalky hydroperoxide radical. The temperature sensitive decomposition of the peroxyalky hydroperoxide radical leads to the production of two $OH\cdot$ radicals. This reaction path is representative of the pre-ignition fuel chemistry. Once the heat-release of the above reactions or the compression process increases the temperature sufficiently high, decomposition of H_2O_2 and peroxyalky hydroperoxide radicals lead to a rapid increase in the number of radicals, further increasing reaction rates and leading to the onset of ignition.

The small alkyl and olefin molecules resulting from the reactions of Figure 1-9 are reduced to methyl (C_1) species in Figure 1-10 via reactions with radicals and oxygen molecules. Figure 1-11 shows the conversion of the methyl species into formaldehyde, carbon monoxide, and finally carbon dioxide. Thus the large hydrocarbon molecules of diesel fuel are broken down in a series of reaction steps to single-carbon sized molecules, which when fully oxidized are emitted as carbon dioxide.

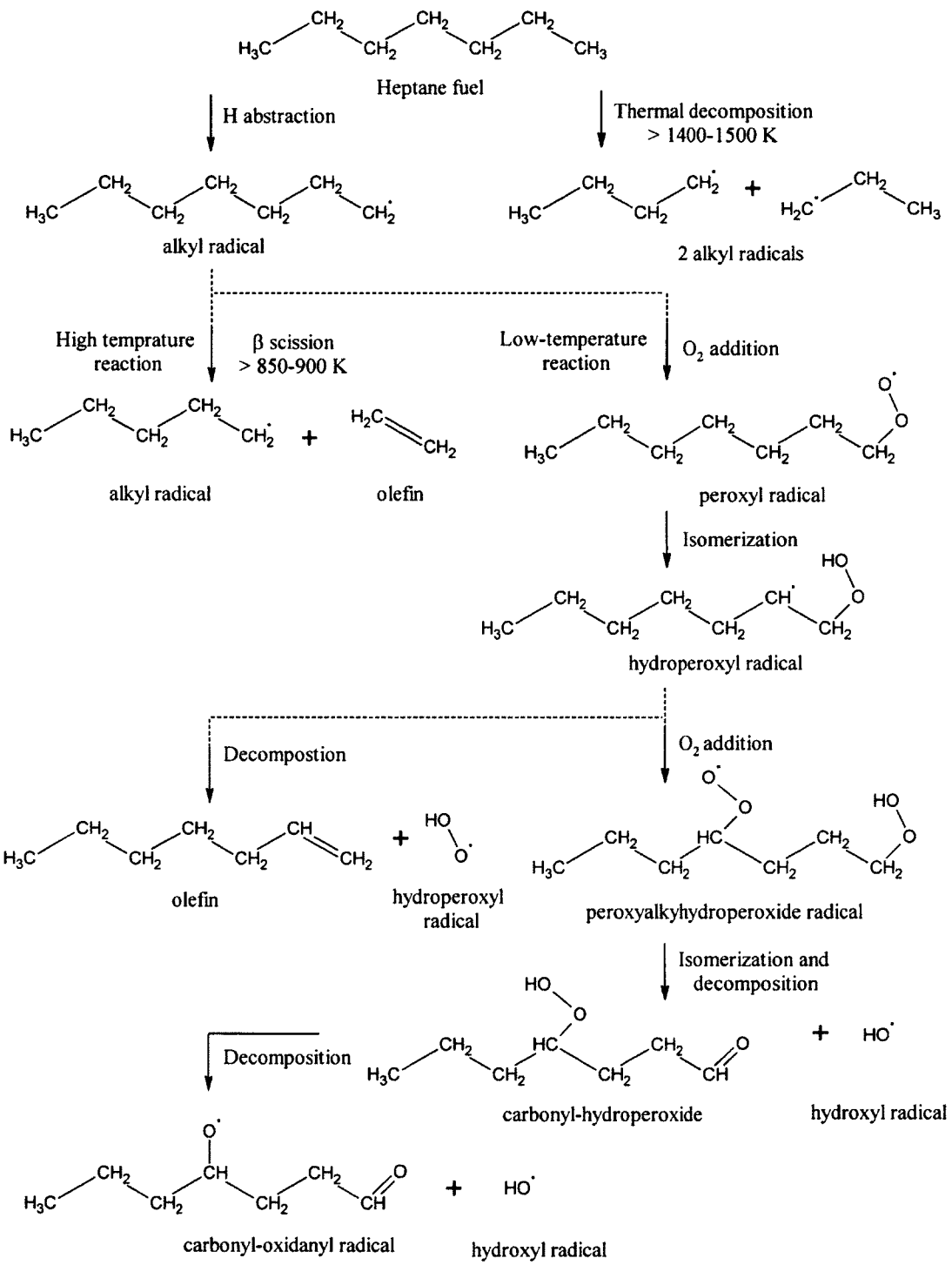

Figure 1-9: Pre-ignition chemistry of heptane fuel

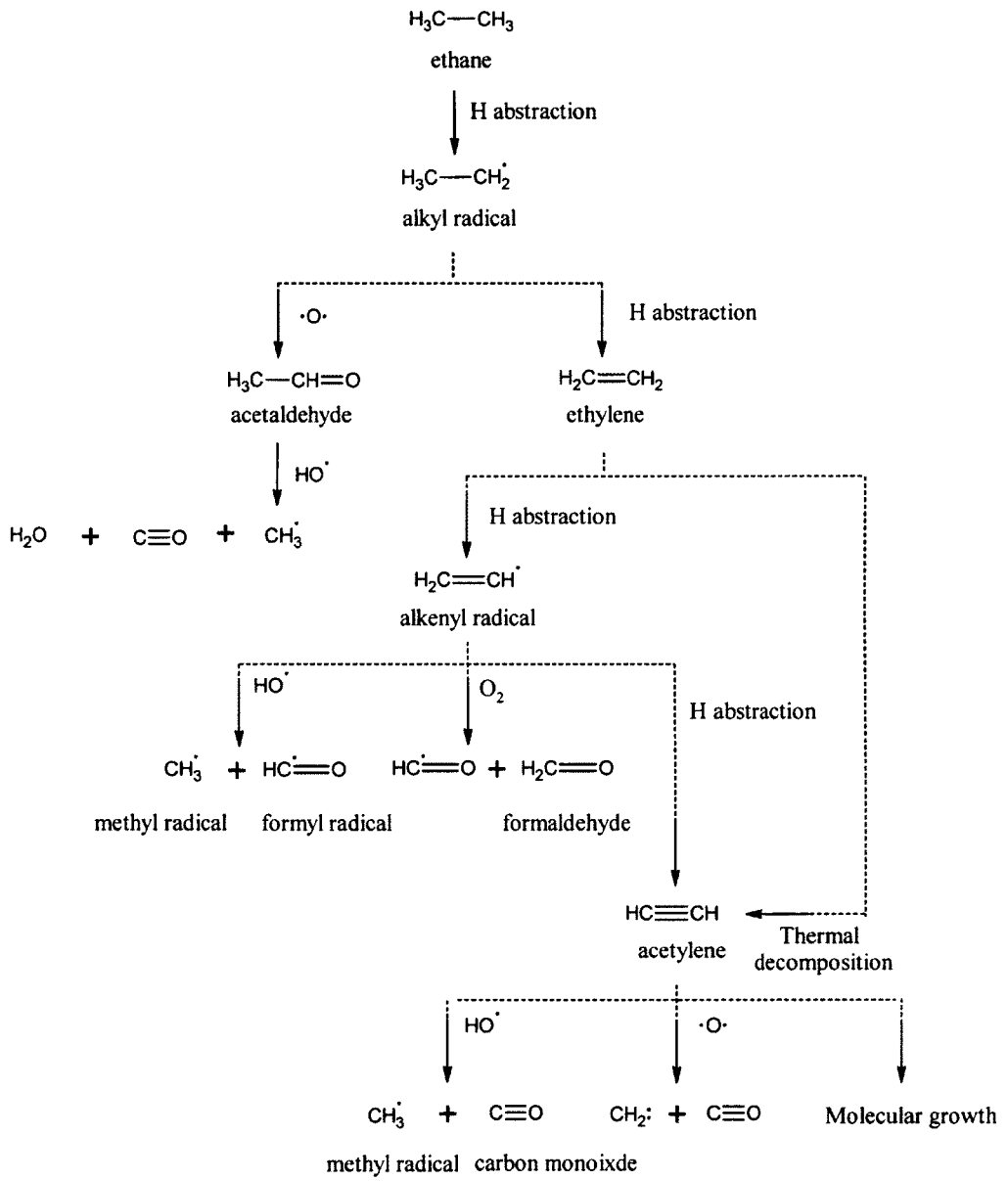

Figure 1-10: Consumption of intermediate small alkanes and alkenes

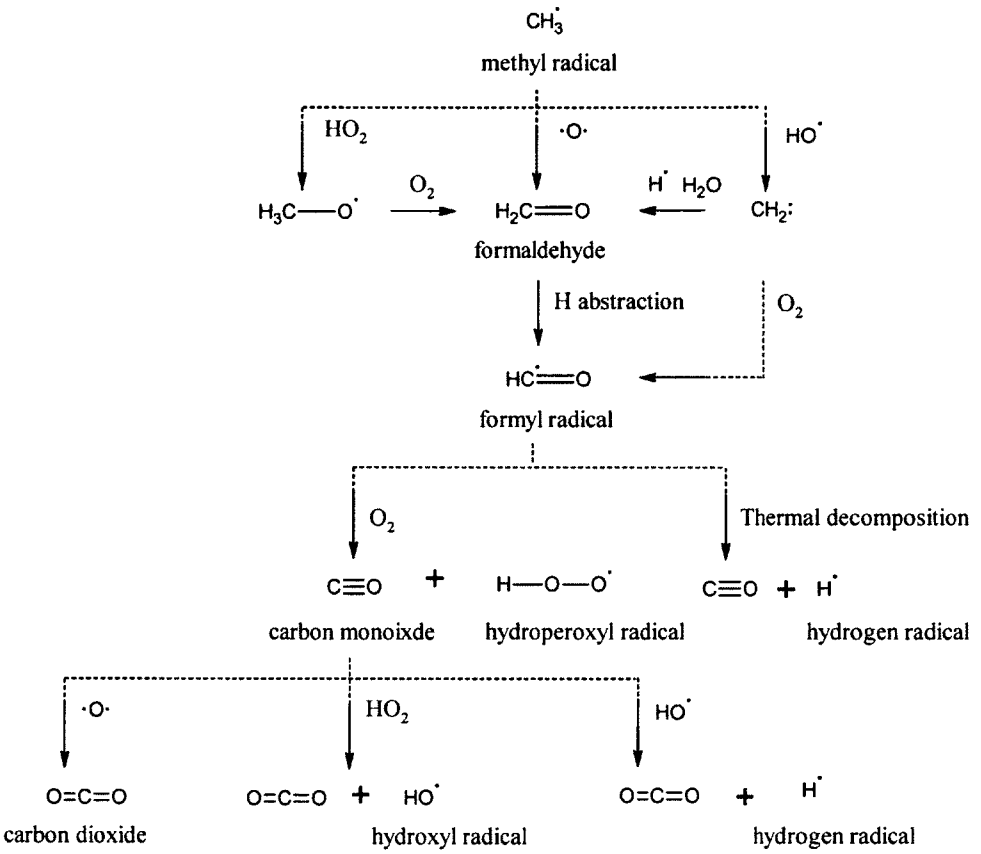

Figure 1-11: Ultimate conversion of fuel carbon into carbon dioxide

1.6 Description of the Diesel Combustion Process

Modern diesel engines employ direct injection of a liquid diesel fuel under high pressures into the hot cylinder air charge. Depending on the fuel injection system type, engine load, and boost level, the injection pressures range from several hundred bars at low load to approximately 2,000 bars at high load for common-rail systems. Higher pressures in the range of 3,000 bars can be achieved for unit injectors and hydraulically intensified injection systems.

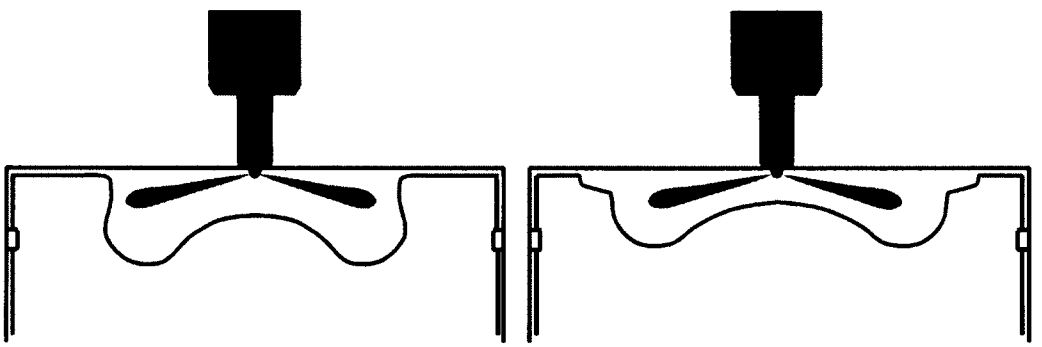

Figure 1-12: Illustration of diesel spray into the combustion chamber

The fuel is delivered through a series of nozzles 0.1 to 0.2 mm in diameter arranged radially around the injector tip, which protrudes into the combustion chamber (Figure 1-12). The spray is shattered by shear forces during the high-pressure injection process, forming a dense cloud of fuel droplets [6]. The droplets undergo evaporation under the compression temperatures as heat is transferred from the surrounding gas to the

liquid. The evaporated fuel is in part carried away from the droplet surface by diffusion and convection, forming mixtures of decreasing richness radiating from the droplet surface [10]. The fuel vapour undergoes the chemistry detailed in the previous section. The ignition tends to initiate in zones where the mixture is near stoichiometric. A diagram of this process is shown in Figure 1-13 below.

If ignition starts prior to complete evaporation of the fuel, a stable flame zone may develop where fuel vapour is continuously transported into the flame zone from the droplet surface and air is transported into the flame zone from the surrounding gas mixture. This is referred to as a *diffusion* or *non-premixed* flame. Under these conditions, the local stoichiometry may approach $\lambda = 1$ even though the global stoichiometry may be significantly lean. The impact of near stoichiometric burning is high flame temperatures leading to high NOx production. In Figure 1-7, adiabatic flame temperatures at $\lambda = 1$ and $\lambda = 2$ are overlaid on the combustion mean gas temperature. While the mean temperature does not exceed 1500 K and is insufficient for NOx formation, flame temperatures where $\lambda = 1$ are calculated to exceed 2600 K. Dilution of the flame to $\lambda = 2$ reduces the flame temperature to under 2000 K, closer to a low-NOx condition. Thus delaying the ignition to allow more time for evaporation of the fuel and mixing with air or recirculated exhaust is a necessary measure to control NOx production in diesel engines.

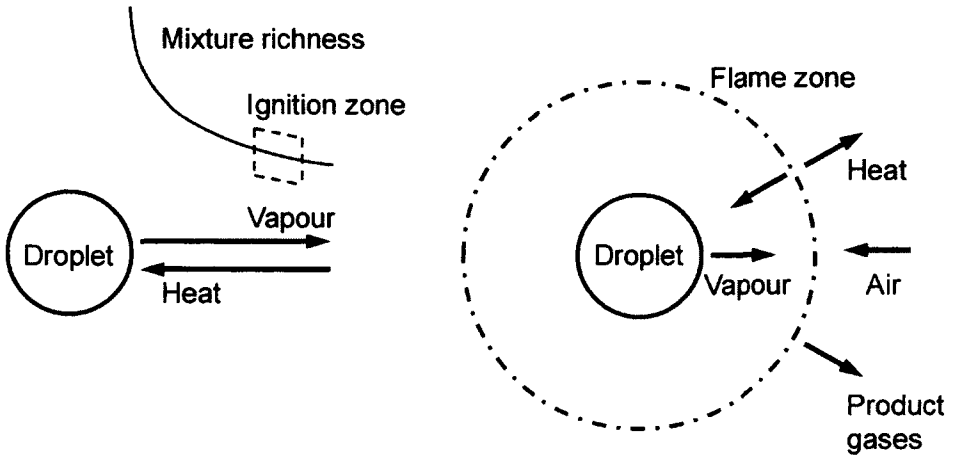

Figure 1-13: Conceptual illustration of fuel droplet evaporation and combustion

1.7 Motivation for Hydrocarbon Speciation

The in-cylinder strategies for NOx reduction introduced in the previous sections aim to achieve low-temperature combustion. However, low-temperature combustion typically has the consequence of increased hydrocarbon emissions. Complete combustion requires the presence of sufficient fuel, oxygen, and temperature. EGR use reduces the oxygen available and lowers the flame temperature. The use of boost increases oxygen availability but can potentially lower the flame temperature. Enhanced mixing can place fuel into regions where wall-quenching inhibits combustion of the fuel or where the mixture is too lean or insufficiently hot for complete combustion.

The products of complete hydrocarbon oxidation are carbon dioxide and water. If combustion is incomplete, partial oxidation products such as carbon monoxide and

formaldehyde are emitted along with partially broken down hydrocarbons such as methane, acetylene, and ethylene. Identification and quantification of the hydrocarbon species emitted can then serve as a diagnostic tool to the in-cylinder processes. Direct measurements of the combustion parameters remain difficult to obtain, owing to high pressures (200 bar), high temperatures (2000 K) and the millisecond order of combustion events. Thus, bulk cylinder pressure and exhaust emission measurements remain as the primary diagnostic tools available.

In the course of tailoring the combustion to minimize NOx production, the additional hydrocarbon emissions can be significant. The hydrocarbon emissions represent a loss of engine efficiency. In addition, they must be treated by the after-treatment system. In the case of less reactive hydrocarbon species such as methane, a gas with a high global warming potential, oxidation may be poor if the exhaust temperature is insufficient for catalytic activity. Thus, practical limits to the effectiveness of the after-treatment system may depend on the engine operating parameter and emitted hydrocarbon composition.

1.8 Objectives of the Study

The objectives of this study are to deploy a set of analyzers and measure in detail the hydrocarbon emissions from low-NOx, low-temperature diesel combustion. The measurement of hydrocarbon emissions is aimed at improving understanding of the in-cylinder phenomena occurring under these engine conditions. Better understanding of the mixing, combustion, and pollutant formation can lead to hardware designs and control strategies that reduce the pollutants emitted and improve the efficiency of diesel engines.

2. REVIEW OF LITERATURE

2.1 Low-Temperature Combustion

The adiabatic flame temperatures of most practical fuels at ambient, stoichiometric conditions exceed the temperature threshold for avoiding NOx production [10]. With the high baseline temperatures encountered in high compression ratio engines, the flame temperatures of stoichiometric mixtures may exceed 2600 K [15], resulting in high NOx production. The principle of low-temperature combustion techniques is to dilute the fuel-air mixture with either sufficient excess-air or recirculated exhaust prior to the onset of ignition. These additional quantities of background gas serve as a local heatsink for the heat released by combustion and lower the flame temperature. In the case of using recirculated exhaust, the lowered oxygen content has the additional effects of delaying the ignition by reducing the oxidation kinetics and decreasing the availability of a necessary reactant for NOx generation.

Low-temperature combustion using diesel fuel is a challenge due to its combination of high ignitability and low volatility. Its characteristic of being relatively slow to evaporate, but igniting rapidly after injection, tends to produce non-premixed burning flames where the necessary dilution is difficult to achieve unless the intake oxygen level is significantly reduced. Implementation of low-temperature combustion with diesel fuel tends to follow either the preparation of a near-homogeneous cylinder

charge with multiple early injections during the compression stroke or with a single injection close to TDC and under heavy EGR. In the multiple early injection strategy, mixing is sufficient but reduced control of ignition timing, high rates of pressure rise, and high HC and CO emissions are consequences of the homogenous nature of the combustion [16, 17, and 18]. A single injection near TDC, with the ignition delayed by heavy use of EGR, can achieve sufficient dilution to reach low-temperature combustion conditions [16, 19, and 20]. The traditionally high thermal efficiency of diesel engines is somewhat compromised by this operating mode [16, 19, and 21]. Furthermore, at high loads excessive smoke levels are an issue.

In contrast to diesel, fuel properties suitable for low-temperature combustion are low ignitability and high volatility. This has led to significant research with the use of fuels alternate to diesel. Dec et al have used gasoline in homogeneous compression ignition engines, using high levels of boost to control the flame temperature and heated intake to control the ignition phasing [22]. Johansson et al have investigated the direct injection of gasoline to achieve partially premixed combustion [23]. Comparisons of combustion with direct injections of diesel, kerosene, and gasoline were done by Subramanian et al [24]. Reitz, Hanson, et al have investigated the use of stratified diesel to modulate the reactivity of a homogeneous gasoline charge [25]. Engine loads of up to 19 bar IMEP have been reported by Eichmeier et al by using diesel-piloted gasoline combustion in a compression ratio 12.5:1 engine [26].

2.2 Hydrocarbon Speciation

The topic of hydrocarbon speciation for diesel low-temperature combustion is not relevantly well reported. When available, published data tend to be limited to light loads conditions or with homogenous type combustion. Koci et al conducted diesel injection timing, injection pressure, and intake pressure sweeps for low-load, high-EGR engine conditions [15]. The load level was 5.5 bars IMEP. Intake oxygen levels were depressed down to 9.5% by heavy use of EGR. The FTIR results indicated that light hydrocarbon (C_1- C_6), along with CO emissions, increased substantially at high EGR levels. This was attributed to local deficiencies of oxygen and decreases in flame temperature. Bohac et al conducted gas chromatography analysis on a diesel engine at compression ratio 16:1 operating in a single injection, EGR diluted low-temperature combustion mode [27]. The load level was approximately 5 bar IMEP. EGR rates of 45% sufficiently controlled the mixing and combustion to achieve low NOx levels. The researchers quantified partially reacted hydrocarbons (i.e. hydrocarbons below the stock fuel size) as 41% of the total hydrocarbon emissions. Methane, ethylene, and acetylene were the only detected species in C_1- C_2 range. As the EGR rate was increased further to 49%, large increases were seen in methane and acetylene emissions and accounted for the majority of increase in the total hydrocarbons.

With respect to homogeneous combustion, Dec et al have performed gas chromatography and liquid chromatography analysis of exhaust hydrocarbons in iso-octane compression-ignition at a compression ratio of 14:1 [28]. Two methods of fuel delivery were tested: a gasoline-type direct injection system and an electrically-heated vaporizer in the intake system. Unreacted fuel was found to be the most prevalent hydrocarbon species for all fuelling strategies, although the quantity was reduced by the use of stratification with direct injection fuelling. As fuelling levels decreased (load levels were not specified), lower bulk temperatures led to increases in emissions of hydrocarbons. The oxygenated hydrocarbons accounted for a significant portion of the total hydrocarbons, ranging from 25% to 40% as fuelling rates decreased. Elghawi et al conducted gas chromatography analysis of gasoline homogeneous compression ignition and similarly found that heavier hydrocarbons (i.e. the stock fuel size range) accounted for approximately 70 to 80% of the total hydrocarbon emissions [29]. The researchers recommended the use of simpler hydrocarbons for further chemical mechanism investigations to avoid the complex chemical nature of the gasoline fuel mixtures. The high levels of fuel-sized hydrocarbon species common in homogeneous combustion in general result from fuel condensation and flame quenching near the engine surfaces.

3. DESIGN AND METHODOLOGY

3.1 Engine Setup

The engine used to conduct this research is a modern common-rail direct-injection single-cylinder research engine. The details of the engine are shown below in Table 3-1 below.

Table 3-1: Engine specifications

Engine Type	Single-cylinder research engine
Displacement (L)	0.74
Bore (mm)	95
Stroke (mm)	105
Injection system	Common-rail piezoelectric direct injection

The engine is coupled to a DC dynamometer through a driveshaft. The driveshaft design uses elastomers its construction to permit limited torsional flexibility. The dynamometer acts as a motor to rotate the engine during no-load or low-load operation and a generator to absorb power from the engine at higher loads. A second function of the dynamometer is to stabilize the engine rotational speed. The rotational speed of the engine fluctuates with-in an engine cycle due to the forces experienced by the piston during the compression and expansion strokes as well as between cycles due to combustion variations. These fluctuations of the engine speed are reduced by the active

response of the dynamometer in conjunction with its added inertial mass and the driveshaft torsional flexibility.

The engine fresh intake comprised of dried, oil-less compressed air supplied from an external compressor and conditioning unit. The compressed air is stepped down from the tank pressure of 5.8 bars to the commanded intake pressure through a series of pneumatic and electro-pneumatic regulators. The fresh intake flow rate is measured by a Roots rotary-type positive displacement air flow meter. An intake surge tank is installed downstream of the air flow meter to reduce the effects of the intermittent intake valve action on the accuracy of air-flow measurements. An exhaust surge tank is similarly installed in the exhaust line to reduce the effects of the intermittent exhaust valve action on the build-up of back-pressure and EGR flow.

The EGR flow is driven by the pressure differential between the engine exhaust and intake lines. This pressure differential is built-up by the use of a pneumatic control valve to restrict the exhaust flow. The recirculated exhaust is taken downstream of the surge tank and introduced into the engine intake upstream of the intake manifold. The EGR rate is controlled by modulating the exhaust back-pressure and EGR valve opening. The EGR temperature was moderated in the EGR cooler, a gas-to-liquid heat-exchanger circulating water or engine coolant. The schematic of the engine air system is shown in Figure 3-1. An alternative EGR configuration to the setup described above is shown in dashed lines, where the surge tank is bypassed for the recirculated exhaust. An advantage

of this short EGR loop is faster EGR response, but with potentially increased engine cycle-to-cycle variations.

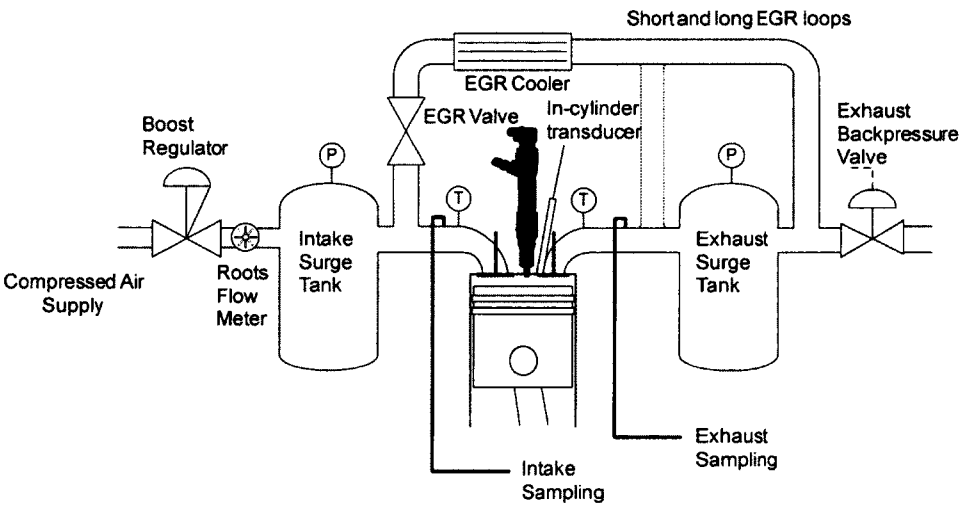

Figure 3-1 Engine air system schematic

The diesel fuel to the engine high-pressure pump is supplied by a gravity-feed tank. A Rheonik RHM 015 coriolis-effect meter and an Ono Sokki FP 213 piston-method volumetric flow detector are used to measure the fuel consumption rate. Five fuel filters are installed for the protection of the flow meters and fuel injection equipment and to improve the measurements. The common-rail high-pressure pump used is a Continental (formerly Siemens VDO) K16 pump, belt-driven from the crank-shaft by a pulley at a reduced ratio of 1.2:1. The high-pressure output from the pump is supplied to a common-rail. One port of the common-rail is used to supply fuel to the injector. Fuel-

return from the injector is routed through the cylinder head and joins the fuel-return from the high-pressure pump. The returned fuel is cooled in a heat-exchanger and then reintroduced into the high-pressure pump supply. The common-rail is instrumented with a piezoelectric pressure transducer. The fuel system is instrumented with thermocouples to measure the temperatures of the fuel supply, injector body, injector return fuel, combined return fuel, and post heat-exchanger combined return fuel. The schematic of the engine fuel system is shown in Figure 3-2 below.

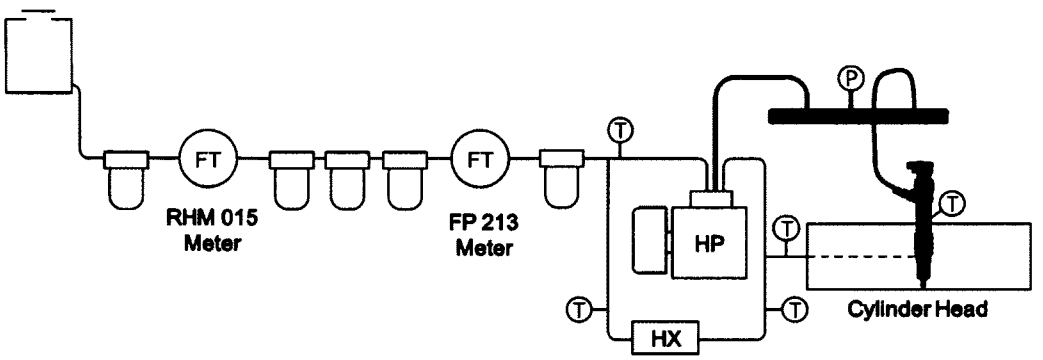

Figure 3-2: Engine fuel system schematic

The cylinder is instrumented with a piezoelectric pressure transducer (Kistler 6052C, 18.9 pico-coulombs per bar sensitivity, 0 to 250 bar range). The transducer is mounted via an adapter sleeve in place of the engine glow plug. The transducer output is converted to a 0-10 V signal by a charge amplifier (Kistler model 5010). The engine position is indicated by a rotary incremental encoder (Gurley Precision Instruments 9124S03600H5L01) at 0.1° resolution. Additional Hall-effect sensors pick up fly-wheel

and cam disk readings to indicate the firing sequence for the engine. The in-cylinder pressure is sampled by a National Instruments PCI-6024E data-acquisition card externally clocked by the 0.1° encoder signal.

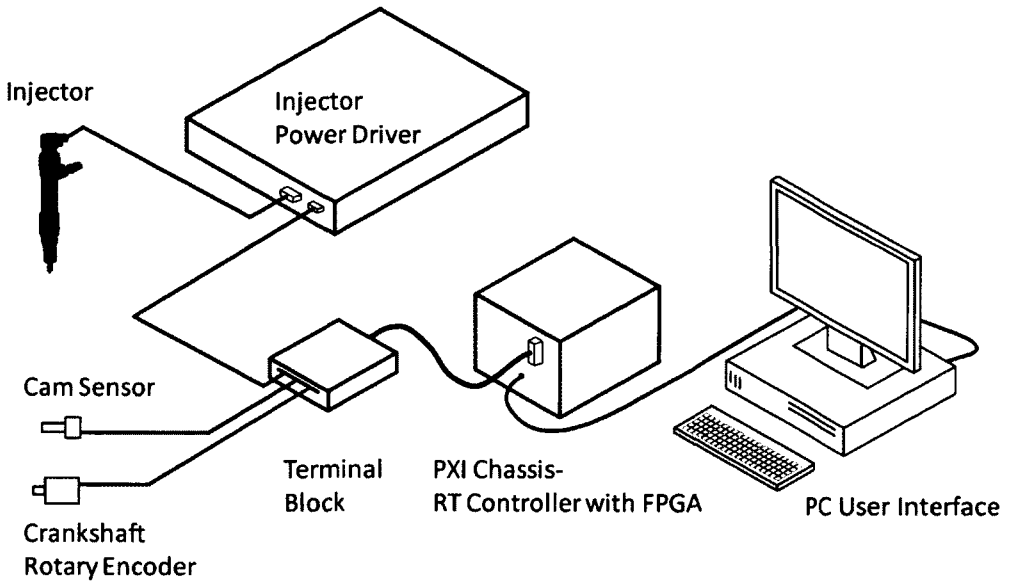

Figure 3-3: Injection control system schematic

The injection control is done by an in-house LabVIEW program deployed on a PXI chassis, which is equipped with a real-time controller and field-programmable gate array resources. The injection control signal is a 5 volt TTL signal sent to a piezoelectric injector power driver (EFS 8370 IPoD). The injector driver generates a high-voltage and high-current signal to energize and de-energize the injector piezo stack. A diagram of the injection control hardware is shown above in Figure 3-3.

3.2 Emission Analysis

A set of exhaust emission analyzers was used to quantify the total hydrocarbons (using CAI model 300M flame ionization detector), CO, CO_2, O_2, NOx, and smoke level. The engine intake composition and EGR rate were quantified by using a second set of O_2 and CO_2 analyzers. The molecular hydrogen was measured with an H-Sense magnetic sector mass spectrometer from V&F Instruments, sensitive at ppm and percent levels. The soot levels were measured using an AVL 415S smoke meter. The smoke level is nominally reported as FSN (filter smoke number). The FSN unit is related to mg/m^3 soot emissions by the following correlation [30]:

$$\frac{mg}{m^3} = \frac{1}{0.405} \times 4.95 \times FSN \times e^{(0.38 \times FSN)}$$

A Fourier transform infrared spectrometer was used to allow limited speciation of the exhaust. Fourier-transform infrared spectroscopy (FTIR) uses interferometry to obtain a scan of infrared absorbencies of the sample gas. The absorption of infrared radiation at specific wavelengths is a property of the molecular composition and structure of each species. The FTIR instrument used was a MKS model 2030HS with a 5.11 metre pathlength gas cell and liquid-nitrogen cooled MCT infrared detector. The gas cell, inlet, and sample line were heated to 191° C. The scan range was configured from 600 to 3500

cm^{-1} at 0.5 cm^{-1} resolution and five scan per second speed. Averages of five scans were recorded at one sample per second time resolution.

The quantification of multi-component samples using FTIR requires the selection of a set of species for analysis. A linear combination of the selected species is then computed by the method of least squares to minimize the residuals between the recorded spectra and the calibration spectra of the selected species. The MKS library used contains calibration spectra for 231 species. The analysis method employed used the following 24 species:

1,3-Butadiene	Acetaldehyde	Acetylene
Benzaldehyde	Butane	CO
CO_2	Dodecane	Ethane
Ethylene	Formaldehyde	Heptane
HNCO	Methane	Naphthalene
N_2O	NH_3	NO
NO_2	Pentane	Propylene
Toluene 191C	Urea by-product	Water

In the analysis of hydrocarbons species where absorption bands may overlap significantly, the results are sensitive to the set of species selected for analysis. For instance, the current algorithm cannot consistently resolve benzene from toluene when both species are included for analysis. Consequently the spectrum of toluene is used as a class definition for benzene and its derivatives.

The full equipment suite used is listed in Table 3-2 below. The instrument range is shown in the right-hand column where applicable. In instances where the calibrated range differed substantially from the instrument full range, the calibrated range is also listed.

Table 3-2: Analyzer model number and measurement range

EXHAUST		
Oxygen	CAI 300 paramagnetic detector	0-25%
Carbon Dioxide	CAI 200 NDIR	0-40%
Carbon Monoxide	CAI 300 NDIR	0-5000 ppm
Carbon Monoxide	CAI 600 NDIR	0-10%
THC	CAI 300M HFID	0-30,000 ppm Cal: 3,010 ppm
Nitrogen Oxides	CAI 600 HCLD	0-3000 ppm
Hydrogen	V&F H-Sense mass spectrometer	0-100% Cal: 0-4000 ppm 0-40%
Smoke	AVL 415S	0-10 FSN
Infrared Spectra	MKS 2030HS FTIR	
INTAKE		
Oxygen	CAI 602P paramagnetic detector	0–25%
Carbon Dioxide	CAI 602P NDIR	0-10%

Two parallel gas-conditioning systems, shown in Figure 3-4 below, were used in this work for sampling the engine exhaust. One system filtered the exhaust to remove particulates and condensed moisture from the exhaust using a chiller. The targeted dewpoint of this stream was 2-4° C. This conditioned exhaust is then supplied to the NDIR, CLD, oxygen, hydrogen, and FID analyzers. A FTIR analyzer was used to sample from this conditioning system to measure light hydrocarbon species. A consequence of the water removal is the loss of exhaust species that have higher boiling points (larger molecular hydrocarbons) or high solubility in water (e.g. formaldehyde, ammonia).

A second heated conditioning system line was added for this work with the objective of maintaining the sample temperature at 191° C throughout the sampling system to reduce hydrocarbon condensation and improve speciation measurements. The sampling pump and all filters were temperature controlled. All the major sections of the sampling line were electrically heated. Minor sections of the line utilized thermal insulation. A second FTIR analyzer was installed to sample from this heated conditioning system and used for later experiments for broader hydrocarbon measurements than that capable with the unheated system.

Typical sample gas water content following the condenser as measured by FTIR analysis is 1-1.5%. Sample water content on the heated line is sensitive to both engine load and EGR level. Typical values can be 5% at 4 bar IMEP and 10.5% at 16 bar IMEP.

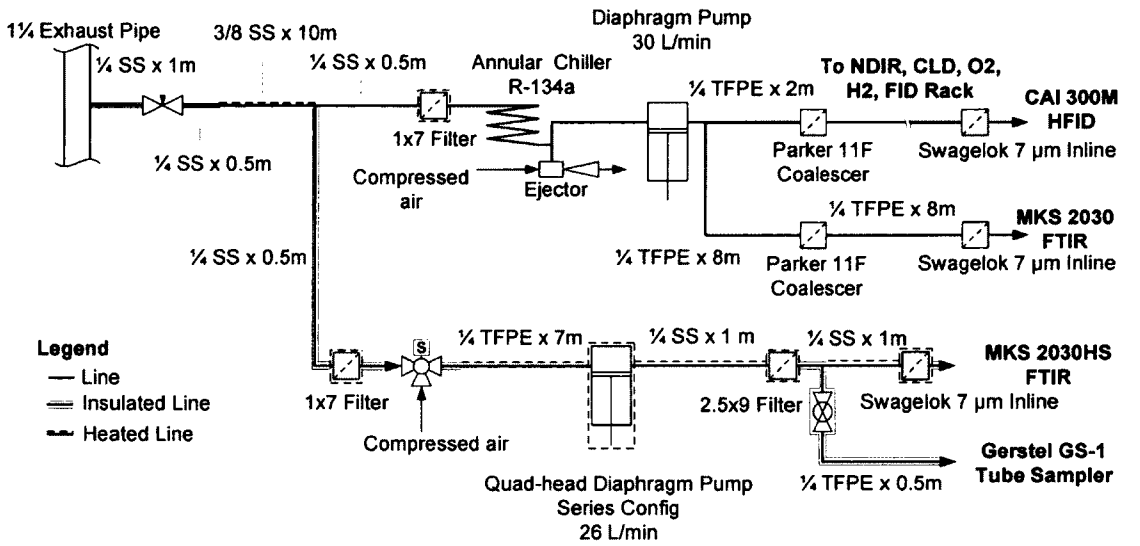

Figure 3-4: Schematic of exhaust emissions sampling train

A gas-chromatographer with a thermal desorption system was set up by the author with the intention of measurement of hydrocarbon species heavier than those possible by the FTIR. The sampling point of this system is located on the heated gas-conditioning system and labelled as Gerstel GS-1 Tube Sampler in Figure 3-4 above. However, due to the extent of calibration work required, quantitative measurements from this instrument were not available at the time of this writing. An overview of the fuel and exhaust hydrocarbon classes and analyzer capabilities is shown in Figure 3-5.

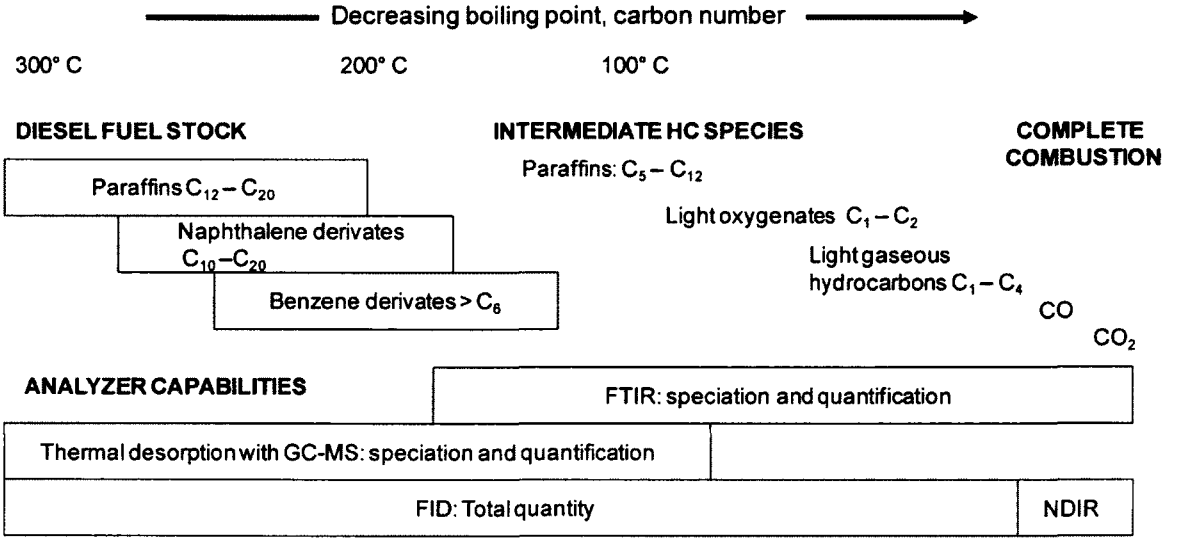

Figure 3-5: Overview of analyzer capabilities for carbon-related measurement

3.3 Experimental Conditions

Results from four series of engine tests are reported in the next chapter. An outline of the conditions in these test series is listed in Table 3-4.

Test Series #1 was a set of EGR sweeps at loads ranging from 5.5 to 18 bar IMEP using single-shot diesel injection. The injection timing was adjusted to keep combustion phasing constant as the EGR was increased. The measure of combustion phasing used was CA_{50} (crank angle of 50% cumulative heat release); CA_{50} was maintained at 372.5° CAD. Test Series #2 studied in detail the effects of intake pressure and common-rail pressure at a constant load of 10 bar IMEP. The CA_{50} was maintained at 370° CAD. The EGR rates applied at theses conditions spanned the full range of EGR application, from zero-EGR, high-temperature combustion to low-NOx, low-temperature combustion. For hydrocarbon speciation, only C_1 – C_2 were reported due the limitations of the cold sampling train in the experiments.

The fully heated hydrocarbon sampling system was available for Test Series #3. These tests were a sweep of engine loads from 4 bar to 16 bar IMEP at moderately-low NOx conditions. The fully heated sampling system allowed quantitative reporting of hydrocarbon species in the range of C_1 to approximately C_{10}. The CA_{50} ranged from 366° CAD at 4 bar IMEP to 396 CAD at 16 bar IMEP. The combustion was retarded to keep the smoke below 2 FSN for these tests. Test Series #4 was intended to supplement Test Series #2 by using the heated sampling system to more fully measure the hydrocarbon

emissions from a sweep of EGR rate at 10 bar IMEP. CA_{50} was maintained at 380° CAD. An open, stepped bowl with a compression ratio of 16:1 was used in the first test series (reference right-hand side of Figure 1-12). The remaining tests used a piston of similar design, but with a reduced compression ratio of 14.3:1. The diesel fuel used was a moderate cetane, ultra-low sulphur certification-grade diesel. Its properties are shown in Table 3-3 below.

Table 3-3: Properties of the diesel fuel used

Density (15° C, kg/ms)	846
Viscosity (40° C, cSt)	2.5
Cetane Number	46.5
Lower Heating Value (MJ/kg)	43.5
Total Sulfur (ppm)	14
H/C Ratio	1.89

Table 3-4: Outline of engine tests reported in this thesis

Test Series	Nominal Load (bar IMEP)	Common-rail Pressure (bar)	Intake Pressure (bar abs)
#1 1600 RPM CR 16:1	5.5	700	1.4
	10.5	1300	2.4
	14.5	1600	2.8
	18	1600	3.2
# 2 1200 RPM CR 14.3:1	10	1200	1.5
	10	1200	2.0
	10	1200	2.5
	10	1500	2.0
# 3 2000 RPM CR 14.3:1	4	1000	1.2
	6	1200	1.4
	8	1500	1.7
	10	1700	2.0
	12	1800	2.2
	14	1800	2.6
	16	1800	3.0
# 4 1600 RPM CR 14.3:1	10	1200	1.8

4. ANALYSIS OF RESULTS

4.1 EGR Application at Various Loads

The effectiveness of EGR application on NOx reduction is shown in Figure 4-1. The NOx emission dropped monotonically with progressively increased EGR (expressed as percentage total engine mass-air-flow, MAF EGR %) at engine loads ranging from low (5.5 bar IMEP) to high (18 bar IMEP). One limitation to the maximum EGR applicable was the incurred smoke penalty. Smoke values exceeding 4 FSN were reached at all but the lowest load. While this level of engine-out emissions can be filtered by the after-treatment DPF, the energy required to regenerate the DPF from the more rapid soot loading is an efficiency penalty on the overall system. Modifying additional combustion parameters such as using multiple injections, increasing the intake pressure, increasing the injection pressure, and delaying the CA_{50} can potentially reduce the smoke levels. The effect of intake and injection pressures will be discussed subsequently in Section 4.2.

The indicated specific fuel consumption (ISFC) for the various engine loads, shown in Figure 4-2, was relatively constant with respect to EGR rates. A slight difference in fuel consumption was seen at low engine load, because of the slightly lower combustion efficiencies and higher relative loss of the combustion energy by heat-transfer. It should be noted that accurate point-by-point fuel consumption measurements

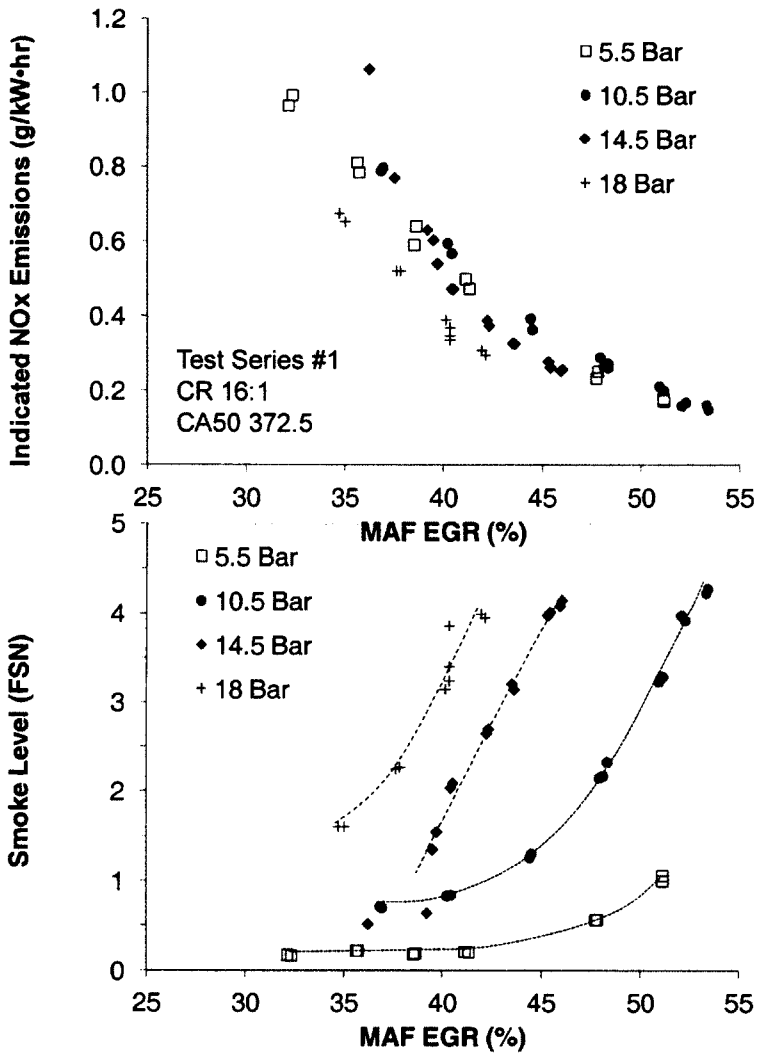

Figure 4-1: NOx and smoke emissions, Test Series #1

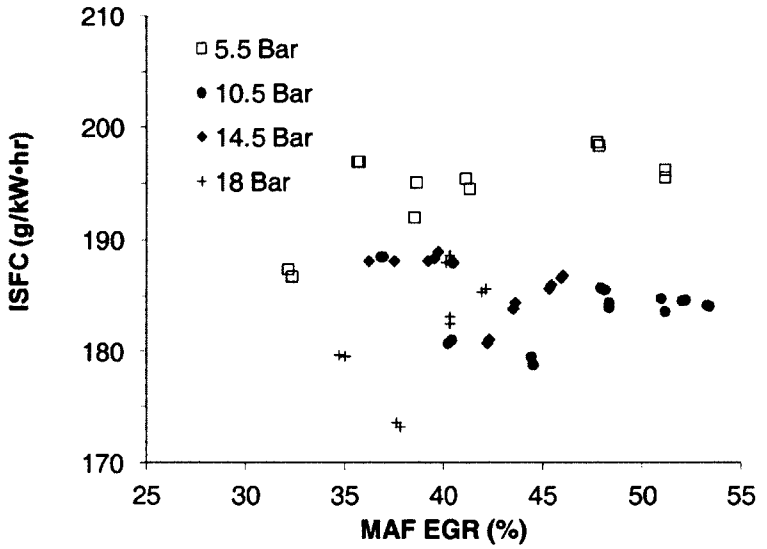

Figure 4-2: Indicated fuel consumption, Test Series #1

in small single-cylinder engines are difficult in general. The measurements are reported here to illustrate the general trends in fuel consumption. Major factors that degrade the measurement are the low rates of flow, the high fuel circulation rate relative to consumption rate (bleed from the high-pressure pump and the injectors), the pulsations caused by to the periodic fuel pumping, and the thermal expansion and contraction of the fuel.

A decrease of combustion efficiency due to the application of EGR is evident in the carbon monoxide and total hydrocarbon emissions, shown in Figure 4-3 below. Carbon monoxide and hydrocarbon emissions represent fuel carbon that has not fully released its chemical potential energy. Of these products, the quantity of carbon

monoxide represented considerably more mass and energy potential than the total hydrocarbons measured by the FID. It was seen that at higher loads the higher mean gas temperatures promoted more complete oxidation and reduced carbon monoxide and total

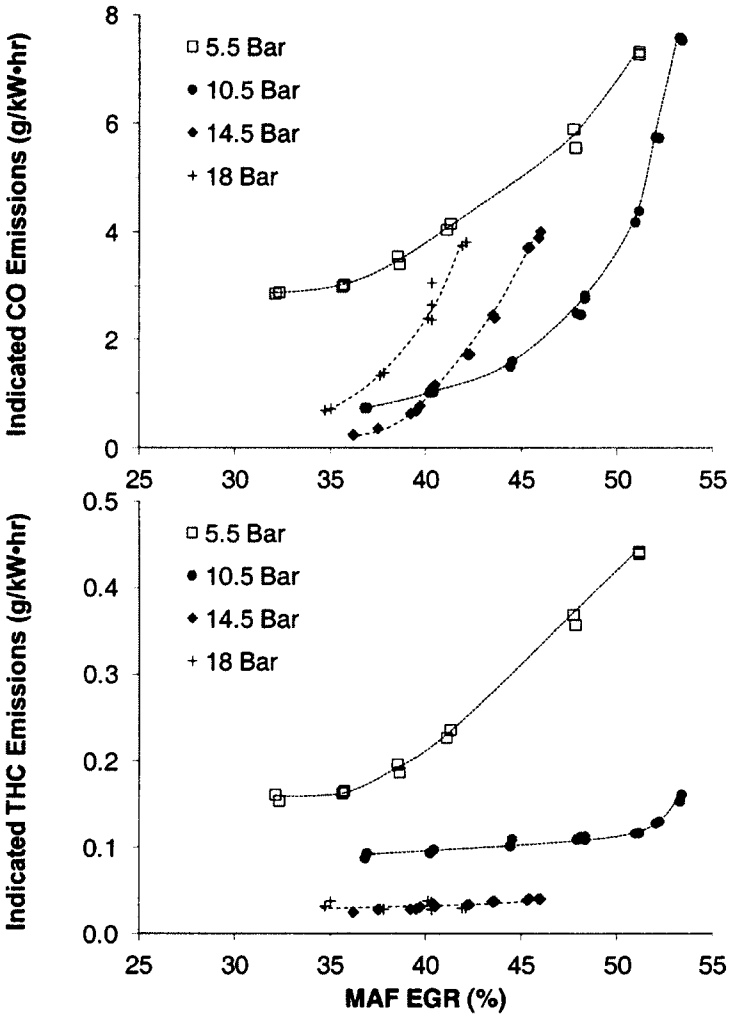

Figure 4-3: Carbon monoxide and total hydrocarbon emissions, Test Series #1

hydrocarbon emissions. A competing effect, however, was the reduction in overall λ at higher loads. This effect was moderated, but not eliminated under such boosted engine conditions. Thus it was seen that the limited oxygen availability caused an increase in the carbon monoxide emissions at 18 bar IMEP relative to mid-load conditions.

The FTIR measurement of the $C_1 - C_2$ hydrocarbon species emitted in the exhaust are shown in Figure 4-4 below. Two general load-related trends are observed. At low loads, the composition of the $C_1 - C_2$ species remained constant, even as their total quantities increased with higher EGR application. The total contribution of methane, ethylene, and acetylene to measured hydrocarbons remained relatively constant at 35%. The distribution along the species was also constant, in the decreasing order of ethylene, methane, and acetylene. At higher loads, the contribution of $C_1 - C_2$ species to the total hydrocarbons was low at moderate EGR rates, but increased significantly at the highest EGR rates. Increases in methane and acetylene were the greatest, while increases in ethylene were moderate.

The trend of $C_1 - C_2$ light hydrocarbons with respect to load and EGR ratios can be explained as the influence of three factors: temperature, mixing, and oxygen availability, prevalent at different conditions. Under low-load conditions, excessive over-mixing can produce pockets too cool or lean for sufficiently fast oxidation. This stochastic process produces hydrocarbons in a wide range of molecular sizes inversely proportional to their degree of oxidation. At higher loads the in-cylinder conditions are

different in several respects. The higher cylinder-charge average temperature kinetically enhances hydrocarbon oxidation rates. With greater fuel quantities injected, a greater portion of the combustion chamber volume is occupied by the air-fuel mixture, so the effect of quenching due to mixing is reduced. The inability the hydrocarbons to be fully oxidized late in the combustion window due to insufficient local oxygen at high EGR

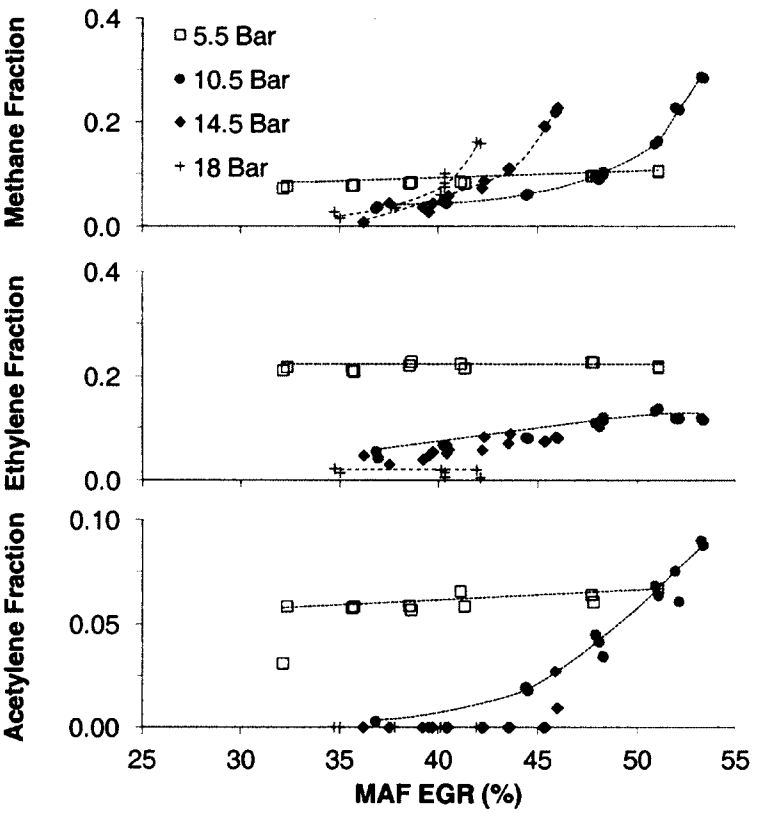

Figure 4-4: Fraction of measured C_1-C_2 species relative to THC, Test Series #1

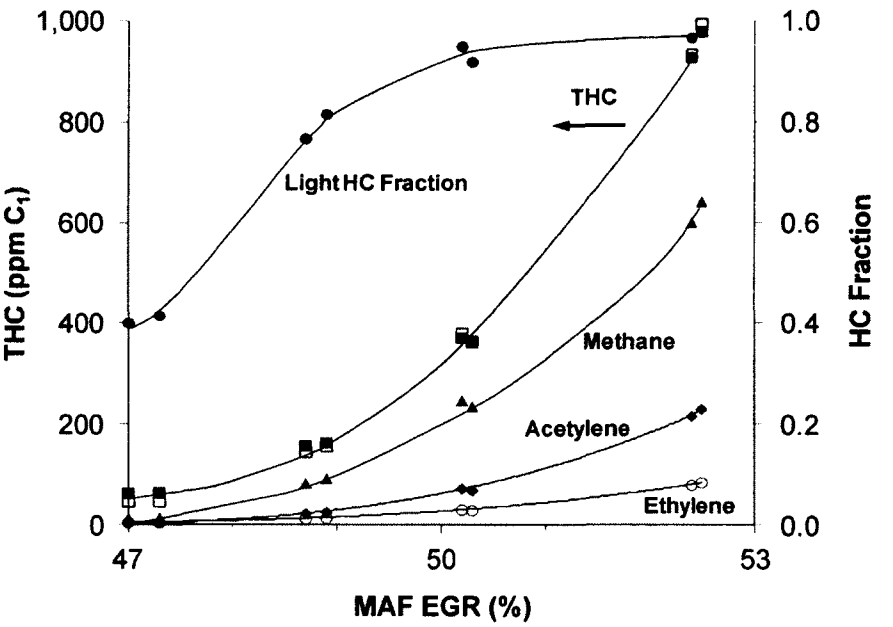

Figure 4-5: Hydrocarbon emissions under high EGR rates at 10.5 bar IMEP

ratios results in the emission of primarily light hydrocarbon species. Since the total hydrocarbon emission at higher loads is reduced, increases in these light hydrocarbons reduce the average hydrocarbon size of the exhaust. Figure 4-5 shows a case of heavy application of EGR at 10.5 bar IMEP and slightly reduced boost (2.0 bar intake) where the $C_1 - C_2$ fraction approach unity.

Measurements of exhaust hydrocarbon emission with a fully-heated FTIR sampling train was performed in Test Series #3 at loads from 4 to 16 bar IMEP. The CA_{50}, ranging from 366° CAD at 4 bar IMEP to 396° CAD at 16 bar IMEP, were generally retarded from timings of optimal efficiency to restrict the smoke under 2 FSN.

The NOx and smoke performance are shown in Figure 4-6 below. At higher loads, the late combustion phasing had a large impact on the engine efficiency, causing the indicated specific fuel consumption to increase significantly as shown in Figure 4-7.

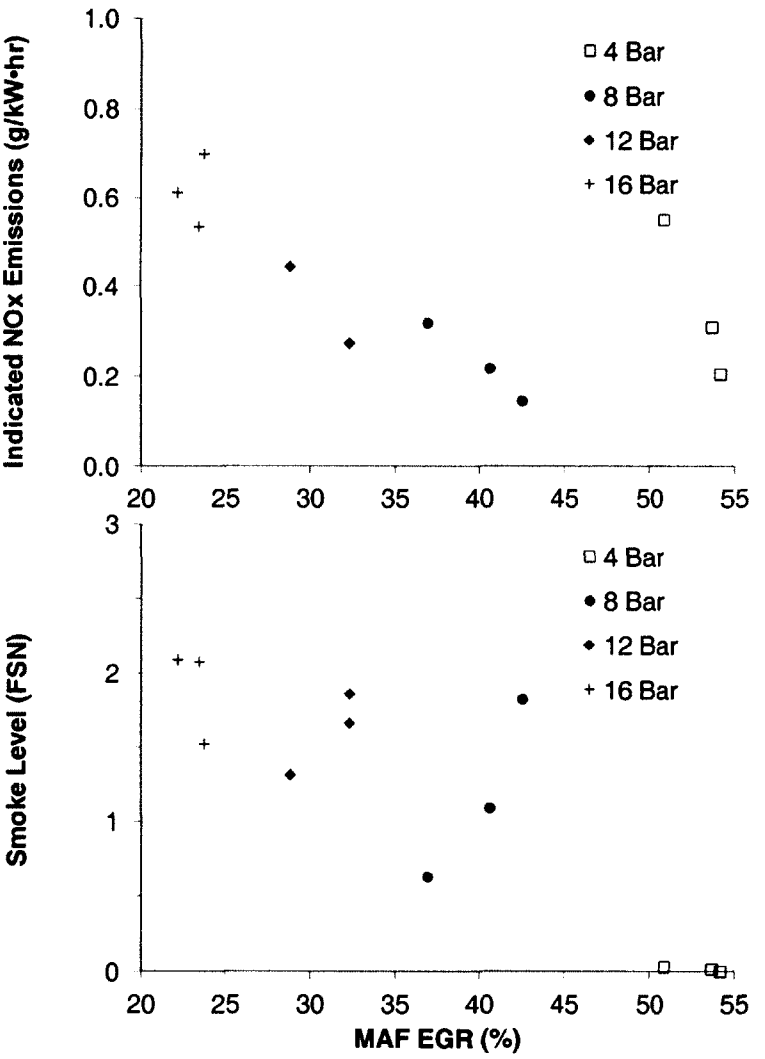

Figure 4-6: Nitrogen oxides and smoke emissions, Test Series #3

In addition, the combination of lower compression ratio (14.3:1) and late combustion phasing in these tests caused high indicated carbon monoxide and total hydrocarbon emissions (Figure 4-8).

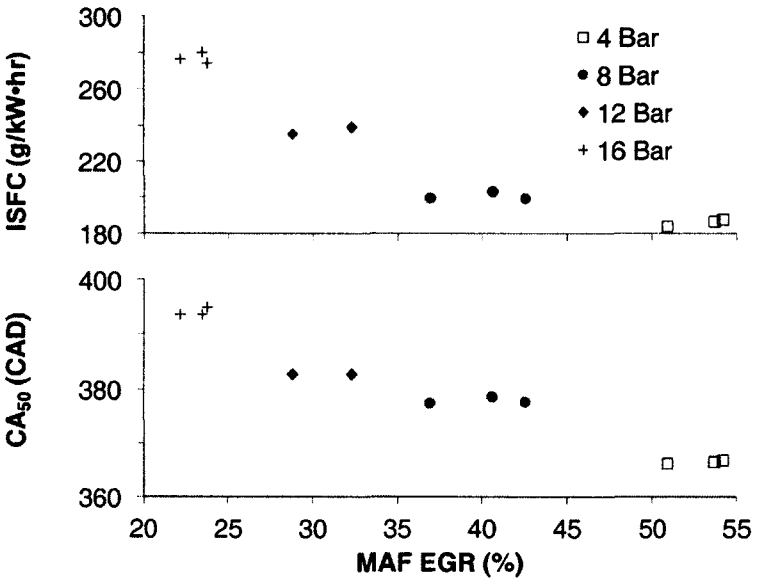

Figure 4-7: Indicated fuel consumption and combustion phasing, Test Series #3

The speciated hydrocarbons, divided into key classes, are shown in Figure 4-9. The $C_1 - C_2$ class comprise of methane, ethylene, and acetylene. The aldehydes includes formaldehyde (CH_2O), acetaldehyde (C_2H_5O), and benzaldehyde (C_7H_6O). The paraffins class represents alkanes in the $C_3 - C_{12}$ range. The aromatics class represents benzene and its derivatives. The span of EGR rates tested at each load is narrow. As a result, few

conclusions about the effect of EGR can be drawn for specific hydrocarbon species. At each load level, the $C_1 - C_2$ class account for the largest portion of hydrocarbons, followed by aldehydes, paraffins, and finally aromatics. The distribution among the classes was relatively similar for all loads except 16 bar IMEP, where $C_1 - C_2$ class accounted for 74% of the measured hydrocarbons.

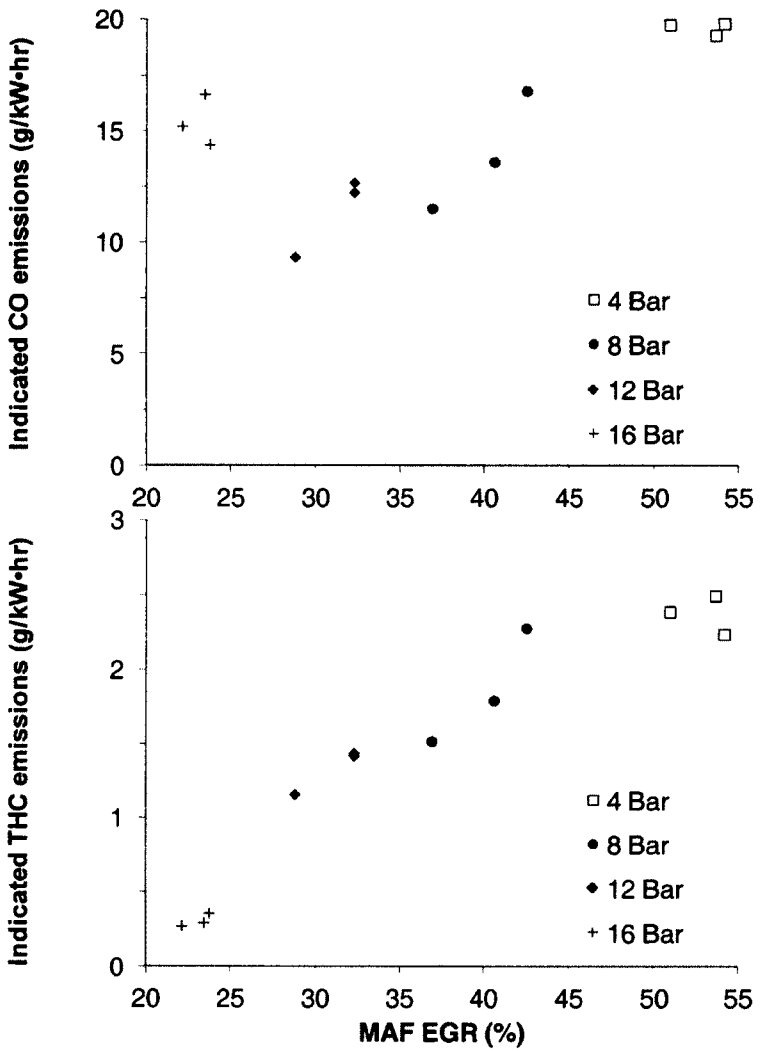

Figure 4-8: Carbon monoxide and total hydrocarbon emissions, Test Series #3

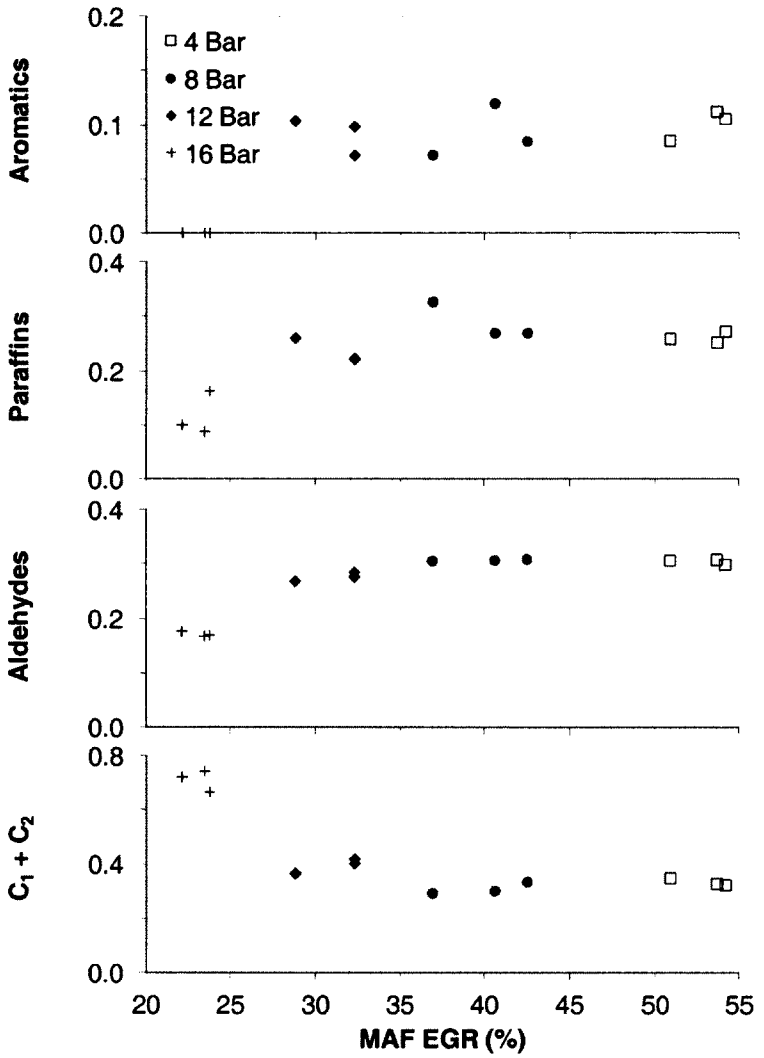

Figure 4-9: Fraction of key hydrocarbon classes, Test Series #3

4.2 Effects of Intake Pressure and Injection Pressure

The isolated effects of intake pressure and injection pressure on diesel combustion are discussed in this section with data from a set of mid-load engine tests at 10 bar IMEP. The intake pressures used were 1.5, 2.0, and 2.5 bar abs. At the 2.0 bar condition, two common-rail pressures were tested: 1200 bar and 1500 bar. The indicated NOx emissions from these tests are shown in Figure 4-10 below.

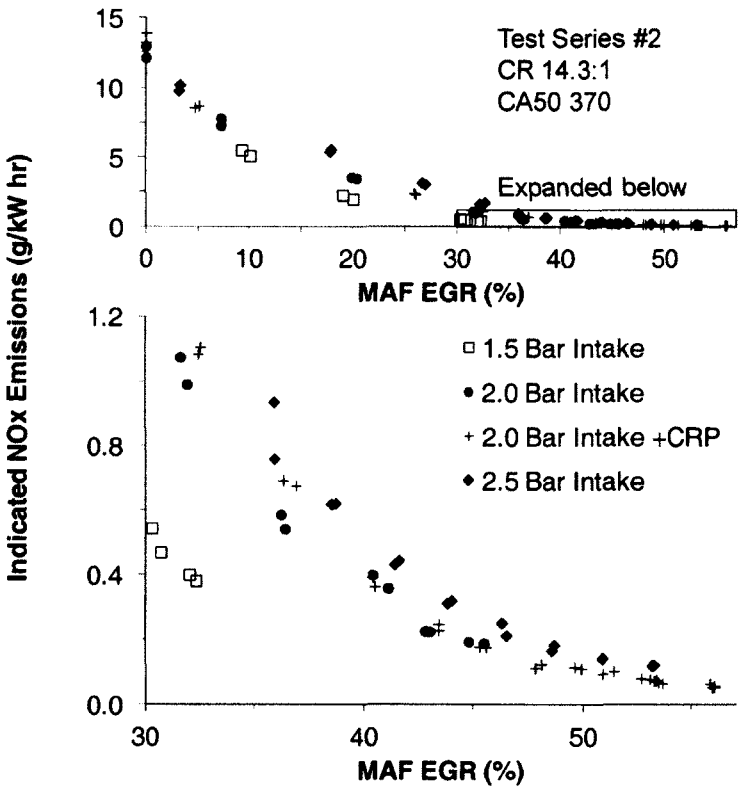

Figure 4-10: Nitrogen oxides emissions from at 10 bar IMEP, Test Series #2

In the absence of EGR-based NOx control, NOx emissions were in the range of 12-14 g/kW hr. NOx performance below 1.0 g/kW hr was achieved with EGR rates of approximately 33%. NOx performance below 0.2 g/kW hr required EGR rates in the range of 45%. The smoke levels were typically seen to increase as a penalty of high rates of EGR application. The tests at 1200 bar common-rail pressure and 1.5 to 2.5 bar intake pressure illustrate this trend in Figure 4-11. Using higher boost pressures was effective in delaying the rise of the smoke levels as well as in suppressing the increase in carbon monoxide and hydrocarbon emissions. Thus higher levels of EGR could be applied to lower NOx prior to reaching unacceptable smoke levels.

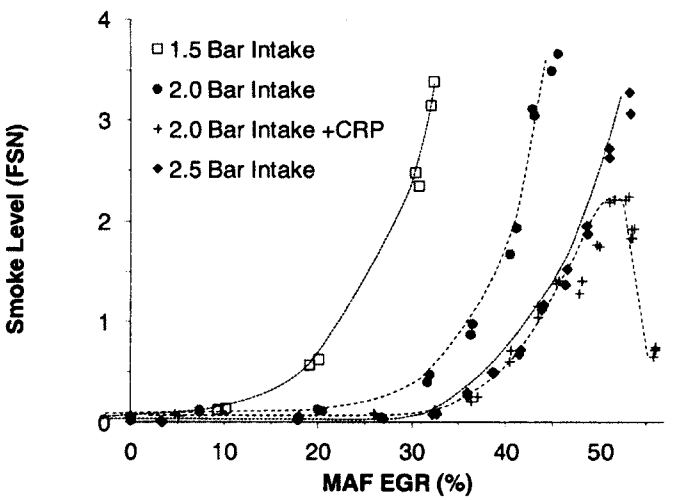

Figure 4-11: Smoke emissions, Test Series #2

Under certain conditions, a simultaneous low-NOx, low-smoke combustion mode can be achieved at very high EGR rates. This was seen in the case at 2.0 bar intake pressure with 1500 bar common-rail pressure (labelled as +CRP). At low to moderately-high EGR rates, the increased injection pressure was effective in reducing smoke levels and to a lesser extent carbon monoxide levels. Hydrocarbon emissions were seen to increase slightly. At EGR rates exceeding 53%, the smoke level was seen to decrease with increasing EGR, contrary to the conventional trend. The conventional description of this behaviour is that as EGR is applied, the increasing ignition delay allows mixing prior to ignition to proceed to a greater extent. In this way, soot production via rich flames is largely avoided. A consequence of this enhanced mixing, as with most homogenous combustions modes, are high carbon monoxide and hydrocarbon emissions. This is shown in Figure 4-12, where carbon monoxide levels reached 37 g/kW hr and measured hydrocarbon emissions reached 1.7 g/kW hr. The impact of these emissions is shown in Figure 4-13, where the indicated specific fuel consumption is graphed against indicated NOx levels. At the very lowest NOx levels, deterioration in fuel economy is significant. The indicated fuel consumption penalties were reduced by the use of higher intake and injection pressures.

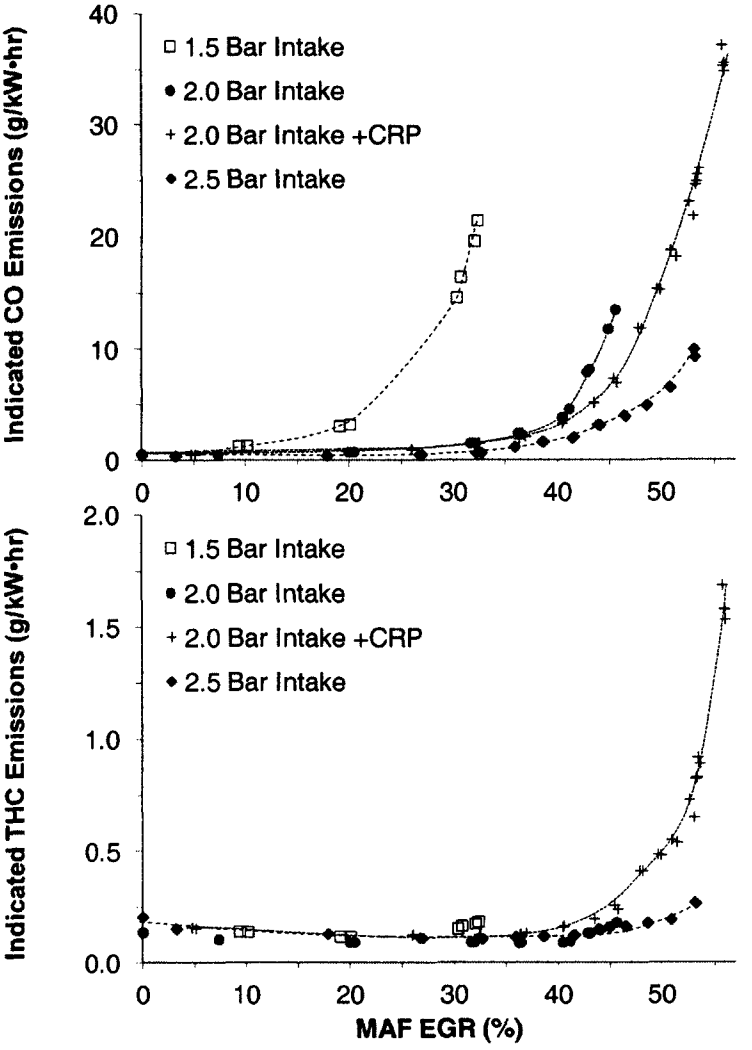

Figure 4-12: Carbon monoxide and total hydrocarbon emissions, Test Series #2

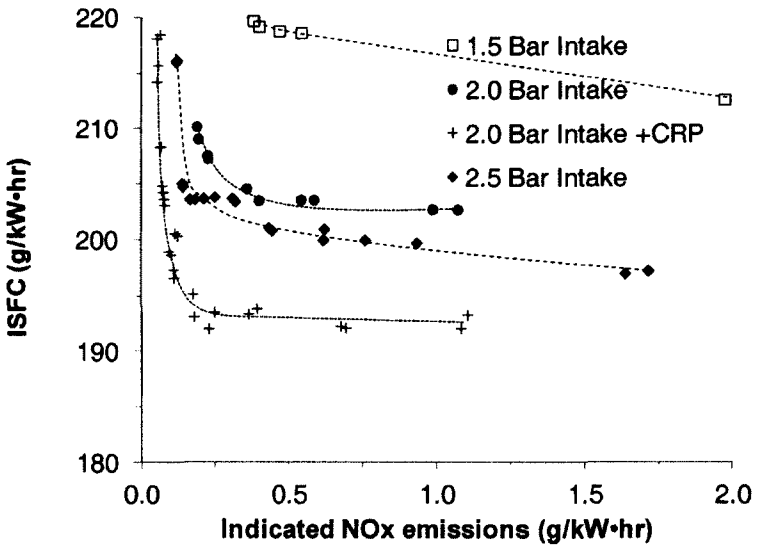

Figure 4-13: Indicated fuel consumption verses NOx levels, Test Series #2

The effect of EGR on mixing is shown in Figure 4-14, where the commanded start of injection, the start of combustion (represented by CA_5, the phasing of 5% heat-release), and the mid-point of combustion are plotted against EGR rate. Up to approximately 25% EGR rate, the change in combustion phasing was minimal. Beyond 25% EGR, the injection timing was advanced to maintain the CA_{50} constant. The start of combustion advanced in response to the change in injection timing, but not at the same rate. The overall effect is that the ignition delay was prolonged. However, it was also seen that the duration of combustion apparently increased, so the overall rate of combustion was slower. Whether the reduced combustion rate is attributable to reduced kinetics at lower flame temperatures and lower oxygen levels or whether the combustion

was still diffusion rate-limited merits further investigation. The high levels of small-molecular hydrocarbons suggest the influence of the latter.

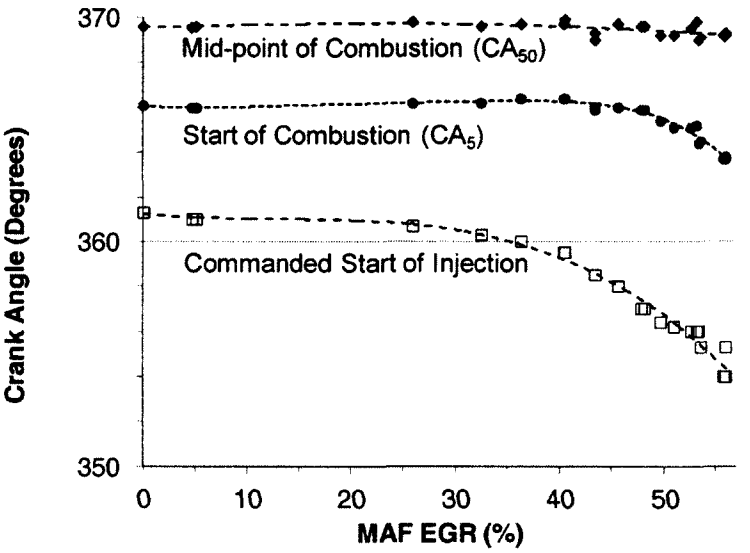

Figure 4-14: Effect of EGR on combustion timings

The FTIR speciation for $C_1 - C_2$ hydrocarbons was done for Test Series #2 and was supplemented by a more complete analysis using a fully-heated sampling system in Test Series #4. $C_1 - C_2$ species were seen to increase significantly with application of EGR. The increase coincided with the increase in total hydrocarbons and accounted for the majority of increase in overall hydrocarbon emissions. As with total hydrocarbons, the increase in $C_1 - C_2$ species occurred under higher EGR rates as the intake pressure was increased. To take into account the increased oxygen quantity available at higher

intake pressures, the $C_1 - C_2$ fraction is plotted against the global λ in Figure 4-15 below. It was seen that while increased boost decreases the total hydrocarbon emissions, the usage of oxygen became less efficient. At 1.5 bar intake pressure, the increase in $C_1 - C_2$ hydrocarbons occurred between λ = 1.24 and λ = 1.45. At intake pressures of 2.0 bar and 2.5 bar, this increase occurred at λ = 1.8 and λ = 2.7, respectively. This suggests that mixing, rather than global oxygen levels, was still predominantly responsible for the hydrocarbon emission characteristics.

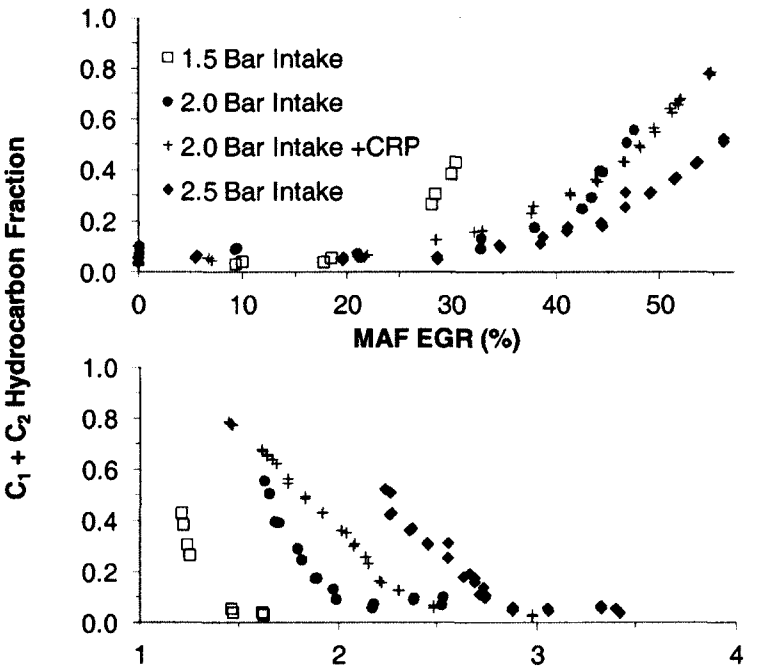

Figure 4-15: C_1-C_2 species plotted against EGR and global lambda, Test Series #2

The contribution of other hydrocarbon classes to the total emissions is shown in Figure 4-16. At low EGR conditions where hydrocarbon emissions were low, moderately sized paraffins accounted for the greatest hydrocarbon fraction. At higher EGR rates, C_1 – C_2 emissions increased rapidly and became the majority of measured hydrocarbons. Increases were seen for aldehydes, paraffins, and aromatics, but their relative contribution were diminished at the highest EGR rates.

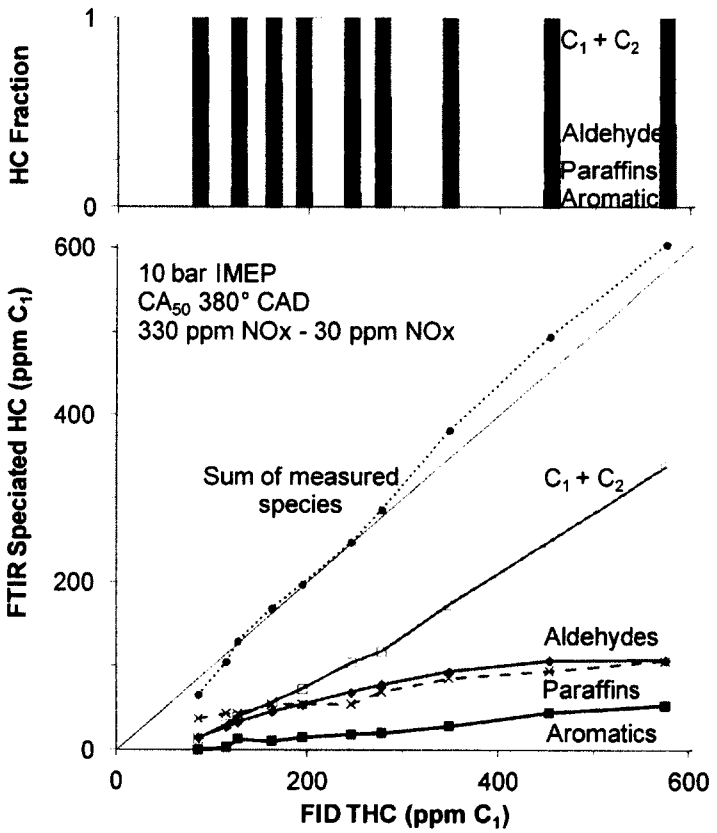

Figure 4-16: Speciated hydrocarbon classes, Test Series #4

5. CONCLUSIONS AND RECOMMENDATIONS

5.1 Hydrocarbon Emissions

In this work, key hydrocarbon species in diesel engine exhaust were quantified with a FTIR instrument. Experimental measurements were undertaken on a modern research diesel engine, under conditions ranging from traditional, high-NOx combustion to EGR-enabled low-NOx, low-temperature combustion. The following conclusions can be drawn from the present hydrocarbon speciation work:

1) The engine load level and EGR rate have strong effects on the total hydrocarbon emissions as well as the composition of the hydrocarbons.

2) At low engine load, as low-NOx, low-temperature combustion is entered via increasing EGR dilution, the total hydrocarbons increase but the composition of the hydrocarbons remained constant. The $C_1 - C_2$ species accounted for approximately 35%, of the total hydrocarbons, indicating a significant amount of heavier species. The large, partially broken-down fuel molecules indicate over-mixing as a cause of the emissions at light loads.

3) At medium and high engine loads, the quantities of total hydrocarbons were generally lower relative to low-load conditions. As the total hydrocarbon emissions increased with increasing EGR application, the composition of the

hydrocarbons changed significantly. At low EGR rates, the hydrocarbon species were predominantly heavier hydrocarbons. $C_1 - C_2$ species accounted for 5 to 15% of the total hydrocarbons, with the large remaining fraction composed of paraffins, aldehydes, and aromatics. As the EGR rates increased, the composition of the hydrocarbons shifted significantly toward $C_1 - C_2$ molecular sizes, with methane and acetylene being the dominant species. The small, late-stage oxidation products indicate the limited oxygen availability under mixing-controlled, high-EGR conditions as the cause of the emissions.

4) At medium engine load, the use of increased injection pressures was effective in reducing smoke emissions, had moderate effect on carbon monoxide emissions, and resulted in higher hydrocarbon emissions. The use of increased intake pressures was effective in reducing smoke, carbon monoxide, and hydrogen emissions, which in turn allowed higher rates of EGR to be applied to further reducing NOx emissions. The effectiveness of oxygen utilization is reduced at higher intake pressures, however. Thus at a high intake pressure of 2.5 bar, even relatively high global λ value of 2.7 could not suppress the increase in $C_1 - C_2$ hydrocarbon associated with high rates of EGR dilution.

5.2 Recommendations for Future Work

This thesis described the measurement of hydrocarbon emissions in diesel low-temperature combustion. While the FTIR was capable of measuring a significant range of hydrocarbons, only very limited detection was possible for hydrocarbons above C_{12}. The application of gas chromatography is necessary for the measurement of larger hydrocarbons in future test programs. Furthermore, the measurement of the total hydrocarbon quantity using a fast-responding FID placed close to the exhaust pipe can potentially avoid condensation losses in the sampling train and provide more accurate quantification.

In the context of the engine, basic concepts concerning the chemistry, thermodynamics, mechanics of the diesel spray and combustion process were presented in the introductory chapter. The integration of the measured engine emissions and these fundamental aspects require significantly more work. For instance, the injector opening and closing dynamics, injector instantaneous fuel flow rate, spray penetration and development, air entrainment, droplet size, and fuel evaporation rate are mechanical aspects of the spray that impact the combustion process. They can be studied through several techniques- injector testing, with rate-of-injection equipment; direct optical, Schlieren, or laser/phase Doppler measurements of the spray in hot, pressurized spray chamber; and through modelling work. The spray ignition behaviour can be studied

inside a combustion chamber under conditions of controlled temperature, pressure, and gas composition. Finally, investigation of the critical mixing-related aspects of diesel combustion can be aided by the use of chemistry mechanisms coupled to fluid mechanical engine models.

APPENDICES

APPENDIX A

FTIR Calibration Spectra

The single species calibration files used for FTIR quantification were supplied by the instrument manufacturer MKS. Typically each calibration file contained several infrared spectra recorded at different concentrations (for example the calibration for methane contained spectra at 20, 40, 60, 80, 100, 210, 414, 623, 1045, 1456, 1897, 2308, 2729, 3143 ppm). The calibration spectra were generated by MKS and third parties using gas standards and dilution systems. Spectra of key species of interest are shown below.

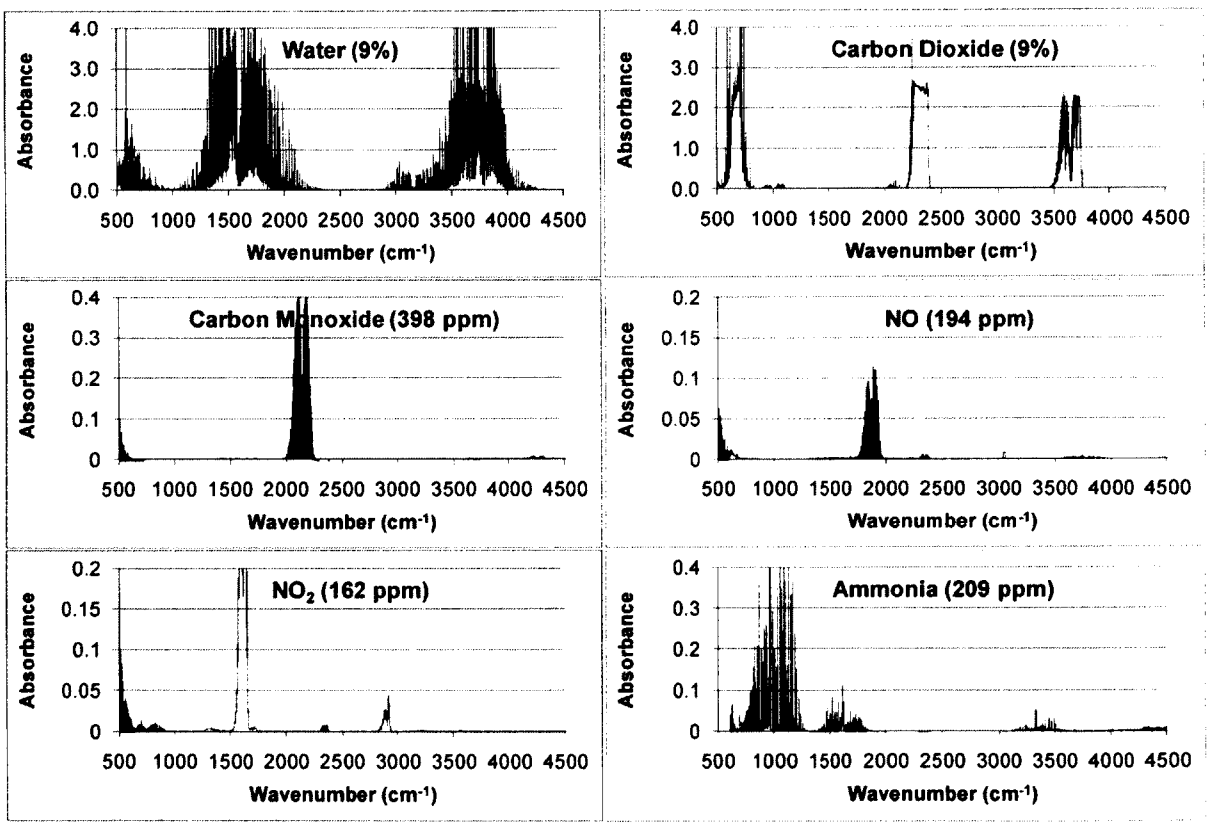

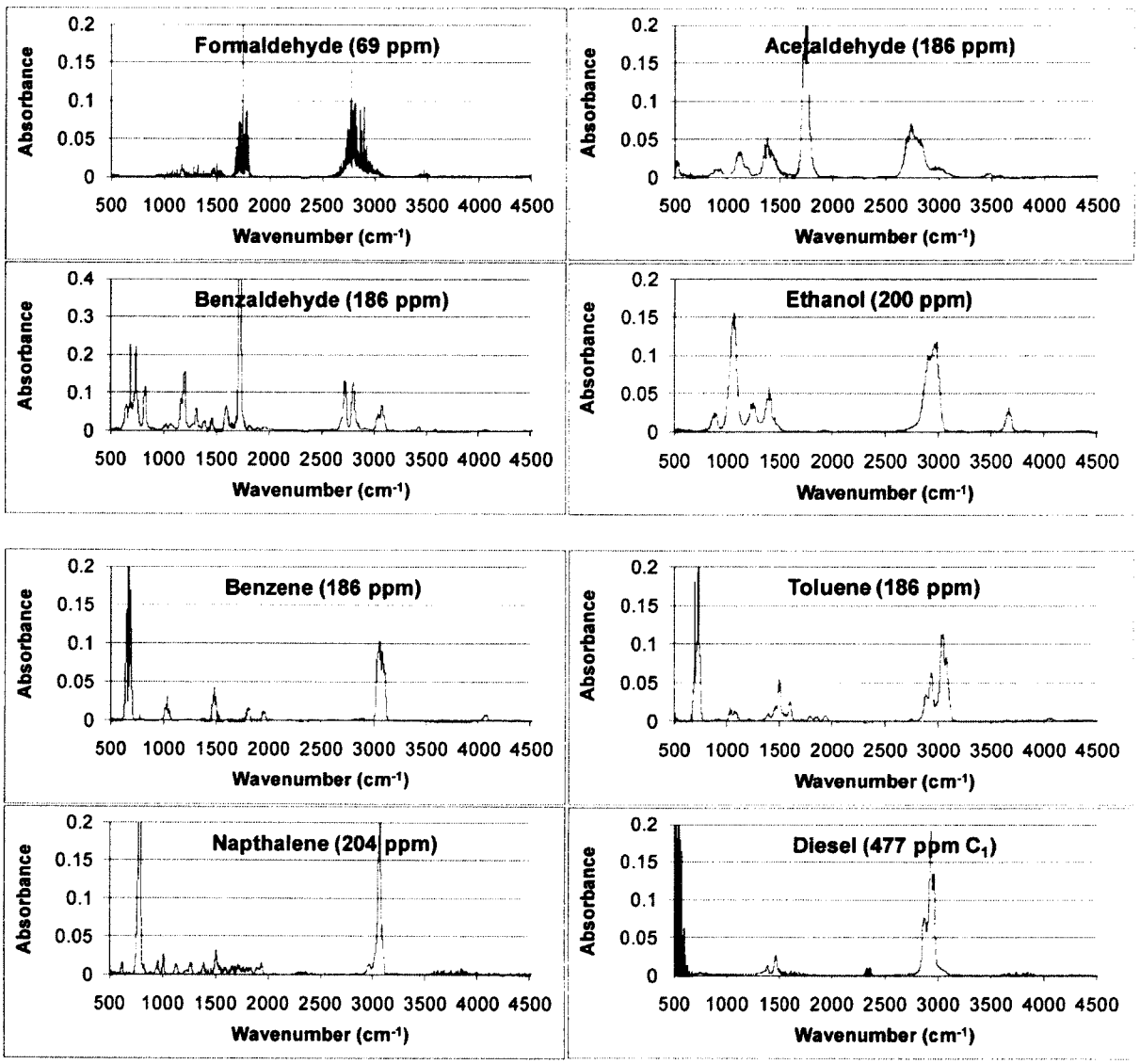
Formaldehyde (69 ppm)
Acetaldehyde (186 ppm)
Benzaldehyde (186 ppm)
Ethanol (200 ppm)
Benzene (186 ppm)
Toluene (186 ppm)
Napthalene (204 ppm)
Diesel (477 ppm C1)
Absorbance
Wavenumber (cm-1)

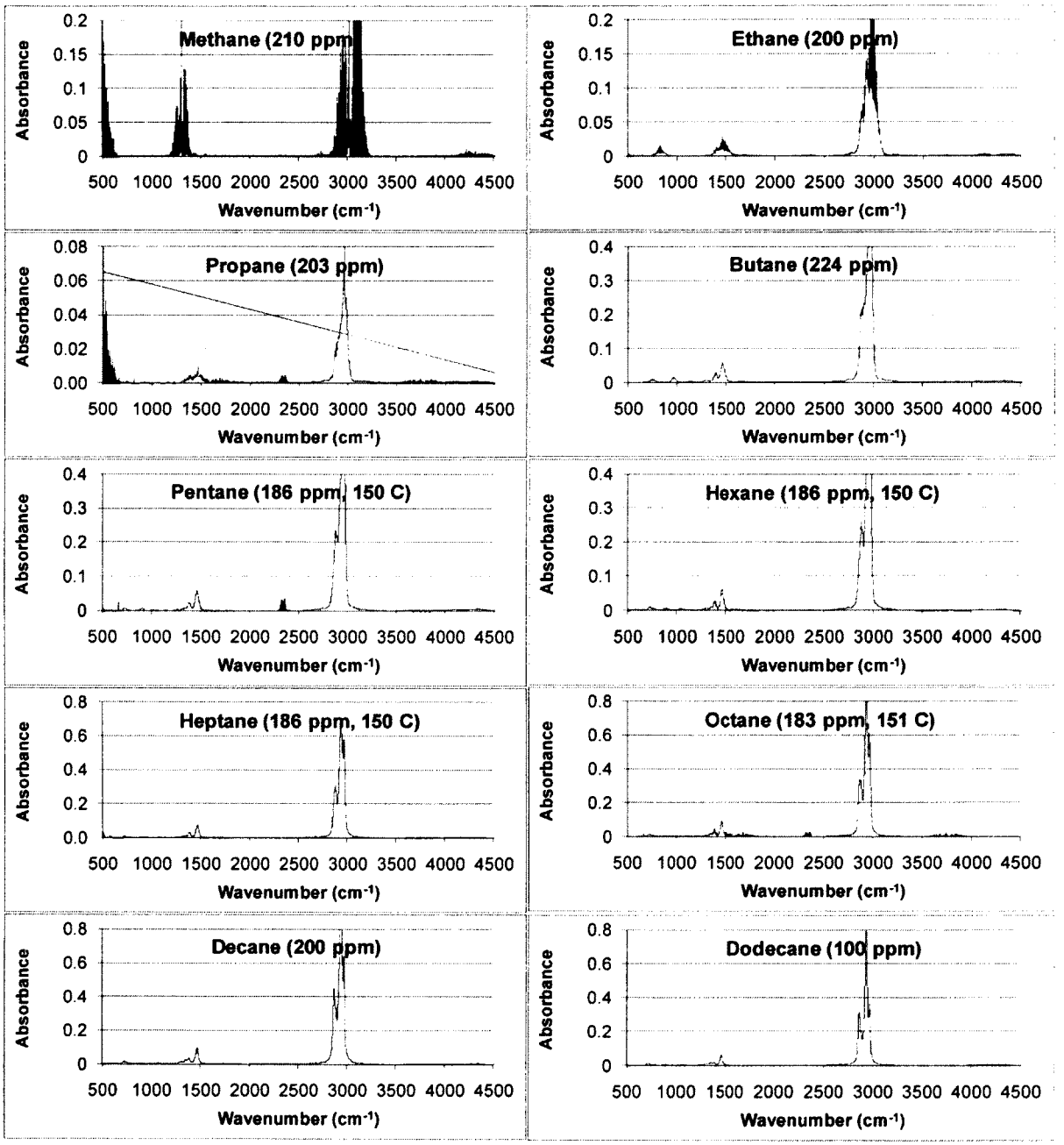
Methane (210 ppm)
Ethane (200 ppm)
Propane (203 ppm)
Butane (224 ppm)
Pentane (186 ppm, 150 C)
Hexane (186 ppm, 150 C)
Heptane (186 ppm, 150 C)
Octane (183 ppm, 151 C)
Decane (200 ppm)
Dodecane (100 ppm)
Absorbance
Wavenumber (cm-1)

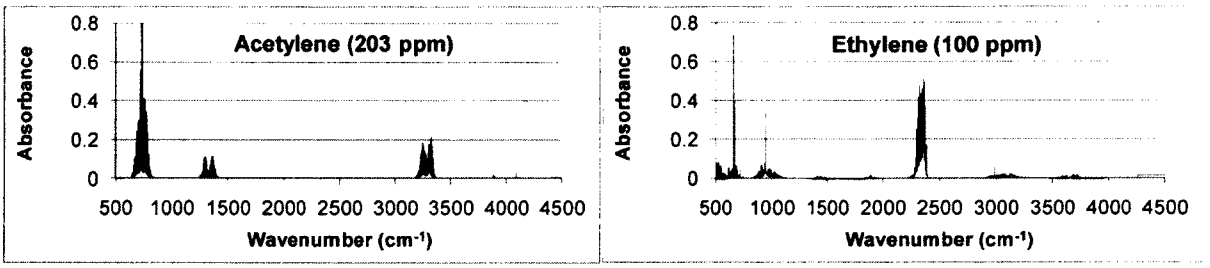
Acetylene (203 ppm)
Absorbance
0.8
0.6
0.4
0.2
0
500 1000 1500 2000 2500 3000 3500 4000 4500
Wavenumber (cm-1)
Ethylene (100 ppm)
Absorbance
0.8
0.6
0.4
0.2
0
500 1000 1500 2000 2500 3000 3500 4000 4500
Wavenumber (cm-1)

REFERENCES

1. Cummins, Lyle. Internal Fire. Wilsonville: Carnot Press, 2000.
2. Cummins, Lyle. Diesel's Engine, Volume One, From Conception to 1918. Wilsonville: Carnot Press, 1993.
3. "CAA National Enforcement Programs." United States Environmental Protection Agency, 2011. Accessed from http://www.epa.gov/compliance/civil/caa/ caaenfprog.html, August 21, 2011.
4. "On-Road Vehicle and Engine Emissions Regulations." Canada Gazette, Government of Canada, Vol 137, 2003. Accessed from http://canadagazette.gc. ca/archives/p2/2003/2003-01-01/html/sor-dors2-eng.html, August 21, 2011.
5. Air Quality Criteria for Ozone and Related Photochemical Oxidants, Vol 1. United States Environmental Protection Agency, 2006.
6. Warnatz, Jurgen. Combustion. Berlin: Springer, 2006.
7. Integrated Science Assessment for Oxides of Nitrogen- Health Criteria. United States Environmental Protection Agency, 2008.
8. *Chemical and Physical Properties of the Fuels for Advanced Combustion Engines (FACE) Research Diesel Fuels.* Coordinating Research Council, 2010. Accessed from

http://www.crcao.com/publications/advancedVehiclesFuelsLubricants/index.html, August 30, 2011.

9. Westbrook, C.K. "Chemical Kinetics of Hydrocarbon Ignition in Practical Combustion System," Proceedings of the Combustion Institute, Vol 28: 1563-1577, 2000.
10. Law, Cheng K. Combustion Physics. Cambridge: Cambridge University Press, 2006.
11. Curran, H.J., Gaffuri, P., Pitz, W.J., Westbrook, C.K. "A Comprehensive Modeling Study of n-Heptane Oxidation," Combustion and Flame, Vol 114: 149-177, 1998.
12. Westbrook, C.K., Pitz, W.J., Herbinet, O., Curran, H.J., Silke, E.J. "A Comprehensive Detailed Chemical Kinetic Reaction Mechanism for Combustion of n-Alkane Hydrocarbons from n-Octane to n-Hexadecane," Combustion and Flame, Vol 156: 181-199, 2009.
13. Curran, H.J., Gaffuri, P., Pitz, W.J., Westbrook, C.K, Leppard, W.R. "Autoignition Chemistry In a Motored Engine: An Experimental and Kinetic Modeling Study," Twenty-Sixth Symposium on Combustion, The Combustion Institute, 2669-2677, 1996.
14. Zheng, J., Yang, W., Miller, D.L., Cernansky, N.P. "A Skeletal Chemical Kinetic Model for the HCCI Combustion Process," SAE Paper 2002-01-0423, 2002.
15. Koci, C.P., Ra, Y., Krieger, R, Andrie, M., Foster, D.E., Siewert, R.M., Durrett, R.P., Ekoto, I., Miles, P.C. "Detailed Unburned Hydrocarbon

Investigations in a Highly-Dilute Diesel Low Temperature Combustion Regime," SAE Technical Paper 2009-01-0928, 2009.

16. Asad, U., Zheng, M., Han, X., Reader, G.T., Wang, M. "Fuel Injection Strategies to Improve Emissions and Efficiency of High Compression Ratio Diesel Engines," SAE International Journal of Engines, Vol 1: 1220-1233, 2008.
17. Kitamura, T., Ito, T. "Mixing-Controlled, Low Temperature Diesel Combustion with Pressure Modulated Multiple-Injection for HSDI Diesel Engine," SAE Technical Paper 2010-01-0609, 2010.
18. Ogawa, H., Miyamoto, N., Shimizu, H. and Kido, S. "Characteristics of Diesel Combustion in Low Oxygen Mixtures with Ultra-high EGR," SAE Technical Paper 2006-01-1147, 2006.
19. Asad, U., Zheng, M. "Efficacy of EGR and Boost in Single-Injection Enabled Low Temperature Combustion," SAE International Journal of Engines, Vol 2: 1085-1097, 2009
20. Kimura, S., Ogawa, H., Matusi, M., Enomoto, Y. "An Experimental Analysis of Low Temperature and Premixed Combustion for Simultaneous Reduction of NOx and Particulate Emissions in Direct Injection Diesel Engines," International Journal of Engine Research, Vol 3: 249-259, 2002.
21. Xie, K., Han, X., Asad, U., Reader, G.T., Zheng, M. "Empirical Study of Energy in Diesel Combustion Emissions with EGR Application," JSAE Technical Paper 20119354, SAE Technical Paper 2011-01-1817, 2011.

22. Dec, J. E. and Yang, Y. "Boosted HCCI for High Power without Engine Knock and with Ultra-Low NOx Emissions Using Conventional Gasoline," SAE International Journal of Engines, Vol 3: 750-767, 2010.

23. Johansson, Bengt. "High-Load Partially Premixed Combustion in a Heavy-Duty Diesel Engine," DEER Conference 2005.

24. Subramanian, S.N., Ciatti, S. "Low Cetane Fuels in Compression Ignition Engine to Achieve LTC," ASME ICEF2011-60014, 2011.

25. Kokjohn, S.L., Hanson, R.M., Splitter, D.A., and Reitz, R.D. "Experiments and Modeling of Dual-Fuel HCCI and PCCI Combustion Using In-Cylinder Fuel Blending," SAE International Journal of Engines Vol 2: 24-39, 2009.

26. Eichmeier, J., Wagner, U., Spicher, U. "Controlling Gasoline Low Temperature Combustion by Diesel Micro Pilot Injection," ASME ICEF2011-60014, 2011.

27. Bohac, S.V., Han, M., Jacobs, T.J., Lopez, A.J., Assanis, D.N., Szymkowicz, P.G. "Speciated Hydrocarbon Emissions from an Automotive Diesel Engine and DOC Utilizing Conventional and PCI Combustion," SAE Technical Paper 2006-01-0201, 2006.

28. Dec, J.E., Davisson, M.L., Sojberg, M., Leif R.N., Hwang, W. "Detailed HCCI Exhaust Speciation and the Sources of Hydrocarbon and Oxygenated Hydrocarbon Emissions," SAE International Journal of Fuels and Lubricants, Vol 1: 50-67, 2008.

29. Elghawi, U., Misztal, J., Tsolakis, A., Wyszynski, M.L., Xu, H.M. "GC-MS Speciation and Quantification of 1,3 Butadiene and Other C1-C6 Hydrocarbons in SI / HCCI V6 Engine Exhaust," SAE Technical Paper 2008-01-0012, 2008.

30. Christian, V.R., Knopf, F., Jaschek, A., Schindler, W. "Eine neue Messmethodik der Bosch-Zalh mit erhohter Empfindlichkeit," Motortechnische Zeitschrift, 54, 16-22.

31. Xie, K., Han, X., Reader, G.T., Wang, M., Zheng, M. "Light Hydrocarbon Emissions from Diesel Low Temperature Combustion," Proceedings of the ASME 2010 International Mechanical Engineering Congress & Exposition, IMECE2010-39191, 2010.

32. Asad, U., Mendoza, A., Xie, K., Jeftic, M., Wang, M, Zheng, M. "Speciation Analysis of Light Hydrocarbon and Hydrogen Production During Diesel Low Temperature Combustion," ASME ICEF2011-60130, 2011.

VITA AUCTORIS

Kelvin Xie was born in Beijing, China. His family moved to the United States and later immigrated to Canada. He studied chemical engineering at the University of Toronto before joining the combustion research program at the University of Windsor.

PUBLICATIONS

In refereed conference proceedings:

Kelvin Xie, Xiaoye Han, Graham T. Reader, Meiping Wang, and Ming Zheng. "Light Hydrocarbon Emissions from Diesel Low Temperature Combustion," Proceedings of the ASME 2010 International Mechanical Engineering Congress & Exposition, IMECE2010-39191, November 16, 2010, Vancouver, British Columbia, Canada.

Kelvin Xie, Xiaoye Han, Usman Asad, Graham T. Reader, and Ming Zheng. "Empirical Study of Energy in Diesel Combustion Emissions with EGR Application," JSAE 20119354, SAE 2011-01-1817, Kyoto, Japan.

Marko Jeftic, Usman Asad, Xiaoye Han, **Kelvin Xie**, Shui Yu, Meiping Wang, and Ming Zheng. "An Analysis of the Production of Hydrogen and Hydrocabon Species by Diesel Post Injection Combustion," Proceedings of the ASME 2011 Internal Combustion Engine Division Fall Technical Conference, ICEF2011-60135, October 3, 2011, Morgantown, West Virginia, USA.

Usman Asad, Arturo Mendoza, **Kelvin Xie**, Marko Jeftic, Meiping Wang, and Ming Zheng. "Speciation Analysis of Light Hydrocarbon and Hydrogen Production During Diesel Low Temperature Combustion," ICEF2011-60130, October 3, 2011, Morgantown, West Virginia, USA.

Shui Yu, **Kelvin Xie**, Xiaoye Han, Marko Jeftic, Tongyang Gao, and Ming Zheng. "Preliminary Study of the Spark Characteristics for Unconventional Cylinder Charge with Strong Air Movement," ICEF2011-60132, October 4, 2011, Morgantown, West Virginia, USA.